Review of Aeronautical Fatigue and Structural Integrity Work in Canada (2019 - 2021)

Authors: **Min Liao**

Report No.:   **LTR-SMM-2021-0120**

RDIMS No.:   **N/A**

Date: **June 2021**

N A T I O N A L   R E S E A R C H   C O U N C I L   C A N A D A   (N R C)

A E R O S P A C E

Review of Aeronautical Fatigue and Structural Integrity Work in Canada (2019 - 2021)

Volume 1 of 1

Report No.:   LTR-SMM-2021-0120

RDIMS No.:   N/A

Date: June 2021

Authors: Min Liao

Classification: Unclassified	Distribution: Unlimited
For:	International Committee on Aeronautical Fatigue and Structural Integrity (ICAF)
Reference:	-
Submitted by:	Dr. Rick Kearsey, Director/A, Structures and Materials Performance Laboratory
Approved by:	Dr. Mouhab Meshreki, Director in General/A, Aerospace Research Center

Pages :	90	Copy No.:	N/A
Figures:	68	Tables:	2

EXECUTIVE SUMMARY

This report provides a review of aeronautical fatigue and structural integrity work carried out in Canada during the period from April 2019 to April 2021. The review is a collection of multiple work summaries that were provided by Canadian industrial partners, universities, and government organizations. All aspects of structural integrity, especially fatigue related work, are covered, including: full-scale testing, aircraft structural integrity program and fleet management, life assessment and enhancement, load and usage monitoring, structural health monitoring, non-destructive inspection, environmental effects, and new material and manufacturing.

This national review will be presented at the first International Committee on Aeronautical Fatigue and Structural Integrity (ICAF) Webinar (https://www.icaf.aero/next_event.php) on June 30th, 2021. The whole report will be archived on the ICAF permanent website (https://www.icaf.aero/index.php).

TABLE OF CONTENTS

LIST OF FIGURES

LIST OF TABLES

Review of Aeronautical Fatigue and Structural Integrity Work in Canada (2019 - 2021)

1.0 INTRODUCTION

Canadian industrial partners, universities and government agencies were solicited for information describing their fatigue technology and structural integrity related activities over the period from April 2019 to April 2021. This review covers work performed or being performed by the following organizations (including some non-Canadian collaborative organizations):

- Bombardier Aerospace (BA)
  - o Aircraft Structural Integration
- L3 Technologies MAS, Inc., a subsidiary of L3Harris Technologies, Inc. (L3 MAS)
- JPWK Aerospace, Canada
- Cranfield University, UK
- Dalhousie University
- École de technologie supérieure (ETS)
- King Saud University, Saudi Arabia
- Laval University
  - o Department of Electrical and Computer Engineering
- National Institute of Technology, India
- Ryerson University
  - o Department of Mechanical and Industrial Engineering
- Royal Military College of Canada (RMC)
- Southwest University, China
- Shanghai Jiao Tong University, China
- University of Alberta
  - o Department of Chemical and Materials Engineering
- University of British Columbia (UBC)
  - o Intelligent Sensing, Diagnostics, and Prognostics Research Lab
- Department of National Defence (DND)
  - o Defence Research and Development Canada (DRDC)
  - o Directorate of Technical Airworthiness and Engineering Support (DTAES)
  - o Quality Engineering Test Establishment (QETE)
  - o Royal Canadian Air Force (RCAF)
- National Research Council Canada, Aerospace Research Centre (NRC Aerospace)

Names of contributors (where available) and their organizations are included in the text of this review. The full addresses of the contributors are available through the ICAF Canadian National Delegate at:

Min Liao, Ph.D., Principal Research Officer
Group Leader - Structural Integrity
Aerospace, National Research Council Canada
1200 Montreal Road, Building M14
Ottawa, ON, K1A 0R6, Canada
Email: Min.Liao@nrc-cnrc.gc.ca

2.0 FULL-SCALE STRUCTURAL AND COMPONENT TESTING

2.1 Global 7500 Durability and Damage Tolerance Tests

Sanjeev Visvanatha, Bombardier Aviation, Aircraft Structural Integration

The Global 7500 Complete Aircraft Durability and Damage Tolerance (DADT) Test started in November 2017 at BAEX (Bombardier Aerospace Experimental Department) in Montreal, Canada. The structural testing was completed in February 2020 after successful completion of the test objectives.

Figure 1 Global 7500 durability and damage tolerance tests in Montreal, Canada

The main objective of the test is to demonstrate the damage tolerance and fatigue characteristics of the metallic components of the Global 7500 airframe as well as to demonstrate no Widespread

Fatigue Damage (WFD) over the Design Service Goal of 17,000 flights. Other objectives include validation of:

1. Crack growth models for primary metal structure
2. Inspection techniques and intervals
3. Typical repairs and allowable damage limits.

The main components covered by the Complete Aircraft DADT Test: complete fuselage, wing, engine mounts, vertical stabilizer and metallic parts of the horizontal stabilizer. It also covers all doors, landing gear interfaces, as well as the control surface and high lift device attachments and backup structures within the wing box and empennage boxes.
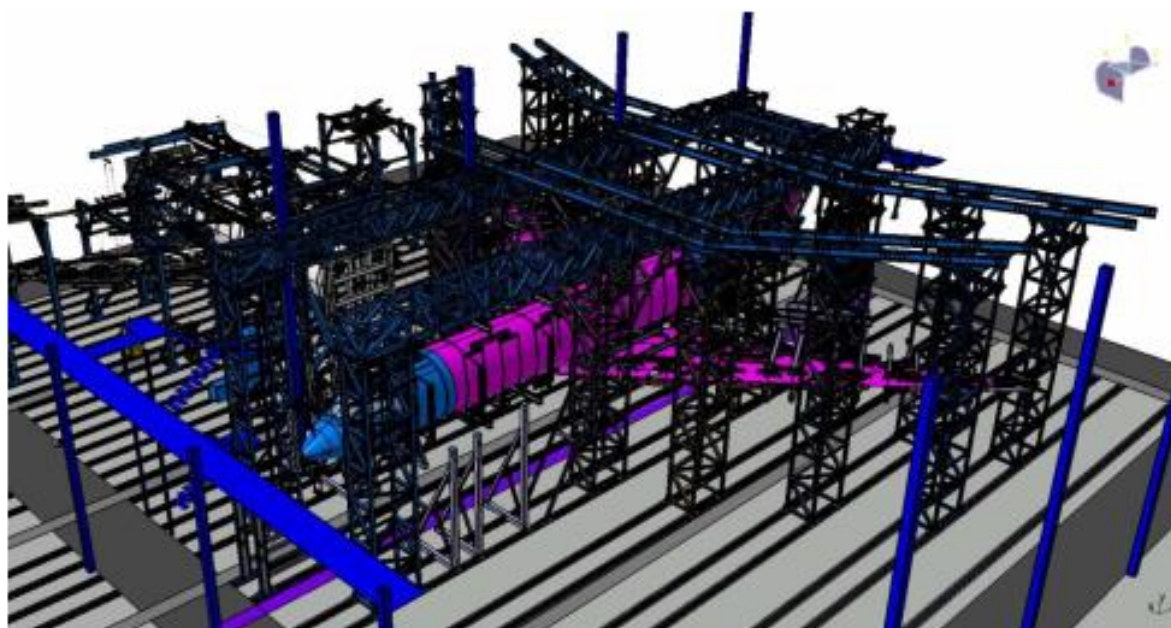
Figure 2 Overall setup of the Global 7500 complete aircraft DADT test

The aircraft structure was subjected to a total of 51,000 flight cycles, which represents three times the Design Service Goal (DSG) of the aircraft. The test program is divided into 3 phases of testing and a final phase for teardown inspection:

1. Phase 1 – Durability testing: Two DSG of flight cycles (34,000 total flights) will be applied to the test article which include typical manufacturing and in-service damage and repairs (Completed).
2. Phase 2 – Damage Tolerance Testing: One DSG of flight cycles (17,000 flights for a total accumulated count of 51,000 flights) will be applied to the test article with the presence of artificial damage at specific PSE locations (Completed).

3. Phase 3 – Residual Strength Testing: A series of residual strength tests will be applied to the test article to demonstrate the structural integrity of standard repairs, confirm the critical crack lengths of the Damage Tolerance Analysis, validate secondary load paths, and demonstrate freedom from Widespread Fatigue Damage (Completed).

4. Phase 4 – Teardown inspection and targeted Widespread Fatigue Damage inspections (Completed).

Figure 3 Close-up of wing test setup

Figure 4 Close-up of fuselage test setup

Three missions with four flight types are applied to the test article. These missions were reduced and truncated to an equivalent of 199 end points, on average, per flight. Number of cycles required for Entry-Into-Service was reached at end of Dec 2017. It completed 2 lifetimes (34,000 flights) of cycling in February 2019. The remaining third lifetime (total accumulated count of 51,000 flights) was completed in July 2019.

After completion of three lifetimes of testing, critical limit load cases were applied in the presence of natural and artificial damage to demonstrate Residual Strength capability of the airframe. Application of limit load cases also allowed demonstration that there was no Widespread Fatigue Damage on the structure. This was completed in February 2020.

In addition, there are multiple Durability and Damage Tolerance (DADT) Bench Tests for components not covered on the Complete Aircraft DADT Test. Below is a list of the main rigs. These bench tests are completed and were tested for 51,000 flight cycles and followed the same testing program as the Complete Aircraft DADT Test.

Table 1 List of subsequent metallic test rigs

TEST RIG (Metallic)
ENGINE MOUNTS (FWD AND AFT) AND THRUST FITTING DADT TESTS
SECONDARY HSTA FITTING DT TEST
ELEVATOR METALLIC COMPONENTS AND REAR SPAR FITTINGS DADT TEST
RUDDER METALLIC DADT TEST
INBOARD FLAP DADT TEST
OUTBOARD FLAP DADT TEST
SLAT DADT TEST
AILERON METALLIC PARTS DADT TEST
SPOILER DADT TEST
WINGLET ROOT JOINT DADT TEST

Both Inboard and Outboard flap Durability and Damage Tolerance Tests are performed at BAEX in Montreal, Canada.

Figure 5 Inboard flap test rig

Figure 6 Outboard flap test rig

Both flaps are moving to various deployment angles during flight-by-flight spectrum to match more accurately interface loads.

As the Global 7500 structure is fabricated utilizing various metal alloys as well as Carbon Fiber Reinforced Plastic (CFRP) for its primary structure, other test rigs are being used to evaluate the durability and damage tolerance characteristics of the composite structure. These rigs are following a different testing program. Below is a list of the main rigs.

Table 2 List of composite test rigs

TEST RIG (Composite)
AILERON STATIC AND COMPOSITE DADT TEST
ELEVATOR STATIC AND COMPOSITE DADT TEST
RUDDER STATIC AND COMPOSITE DADT TEST
HORIZONTAL STABILIZER AND HSTA ATTACHMENTS STATIC AND COMPOSITE DADT TEST

In conclusion, multiple Global 7500 DADT test rigs were completed in support of the Global G7500 Type Certification. Three aircraft design lives (51,000 flight cycles) were simulated to ensure the metallic structure meet the Damage Tolerance certification requirements, the requirements for Entry-Into-Service as well as customer expectations.

2.2 F/A-18 Outer Wing Front Spar Maintenance Induce Damage Fatigue Test (NRC/RCAF/L3 MAS)

Eric Dionne, NRC Aerospace

The NRC Aerospace Research Centre is currently fatigue testing an outer wing that was modified by L3 MAS (L3 Technologies MAS, Inc., a subsidiary of L3Harris Technologies, Inc.) to solve the majority of the Maintenance Induced Damage (MID) found on the CF-188 fleet outer wing (Section 3.1.2). The test article is designated as FT390 and has accumulated 4,572.8 CFH (component flight hours) of in-service usage prior to modification incorporation. This test article was selected because it had MID and no fatigue cracks, which was representative of the majority of the fleet findings. More details of the MID and blend repair by L3 MAS are described in Section 3.1.2.

The front spar area near the OLEF transmission lugs MID is likely originating from the use of unapproved tools to remove sealant. This MID is located in an area where stress risers already exist, which, when combined, will result in a much shorter fatigue life and premature cracking. A blend repair removes MID and very small cracks. Larger cracks are to be addressed via a separate deeper blend that is not addressed by this test.
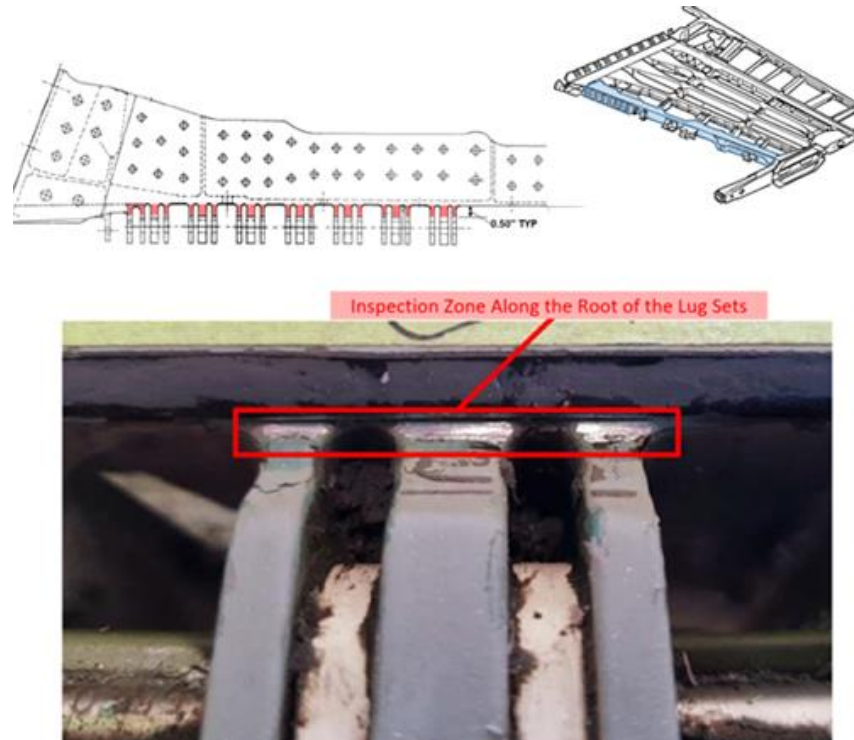
Figure 7 Typical Maintenance Induced Damage and Inspection Area

The aim of this test is to determine the fatigue life of this blend repair, generate crack growth data and demonstrate residual strength. The blend repair will be subject to a maximum of 16909.2 SFH (simulated flight hours) (44 block of 384.3 FH) of fatigue cycling and a 120% Design Limit Load (DLL) demonstration at end of test.

For economical reason, DND chose to recycle an existing Inboard Leading Edge (ILEF) fatigue test rig and incorporate only minor changes. As a result, four jacks on the Outboard Leading Edge Flap (OLEF) were added. The inner wing and outer wing were both installed inverted and connected to a reaction structure. The wing fold and OLEF transmission were both installed to ensure representative load transfer to the test area. The fatigue loads are applied to the upper surface of the OLEF using a push/pull actuator setup. The applied loads are reacted by four jacks installed on the inner wing as well as the reaction structure at the root of the wing.

Figure 8 Test Rig

The spectrum is tailored to match the OLEF hinge moment loads which were shown to be the main stress generator in the repair area. The spectrum also contains different constant amplitude marker block patterns aimed at aiding the derivation of a crack growth curve through quantitative fractography (QF).

OLEF inboard and outboard hinges were both calibrated to determine and validate load transfer into the test area.
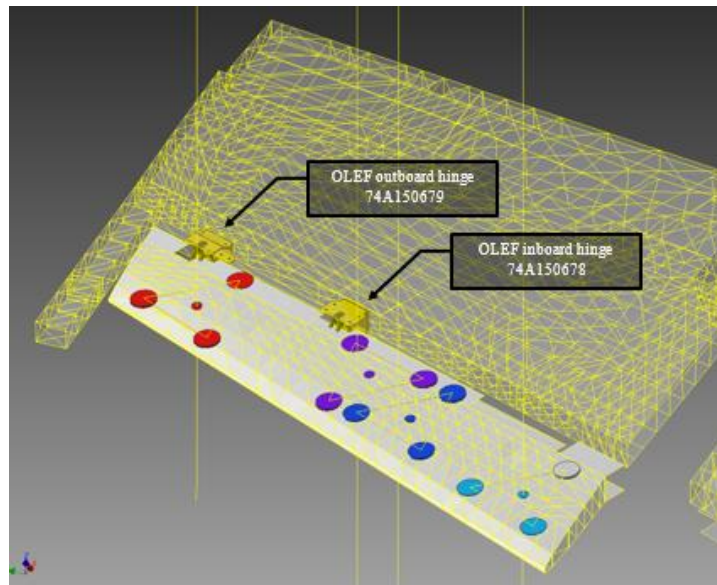
Figure 9 Location of Inboard and Outboard Hinges

The test area was initially inspected via Eddy Current (EC) and RepliSet™. It was then inspected after every block using EC. Monitoring lines were added throughout the spectrum to detect any

trends developing in the strain gauge response. The test article has 30 strain gauges and 6 displacement transducers.

All testing is carried out at the Structural Integrity Laboratory, Building M-14, NRC Aerospace Research Centre, Montreal Road Campus in Ottawa, Ontario, Canada. The fatigue test started in May 2021 and is scheduled to be completed in July 2021.

2.3 F/A-18 Inner Wing Step Lap Joint Residual Strength Test (NRC/RCAF/L3 MAS)

Eric Dionne, NRC Aerospace

The NRC Aerospace Research Centre will perform a static test on a US Navy (USN) wing with a disbond in the lower Step Lap Joint (SLJ). The test article is designated as FT63 based on the inner wing serial number that was donated by the USN. This test is a collaborative project between the RCAF, armasuisse and the US Navy. Other countries participating in the F/A-18 Fighter International Structural Integrity Forum (FISIF) are also contributing to this test.
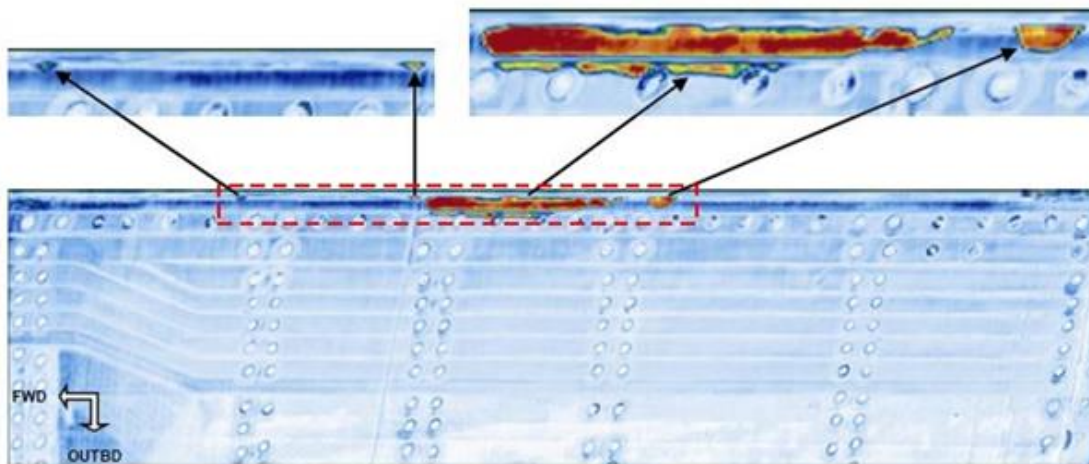
Figure 10 Disbond on Test Article
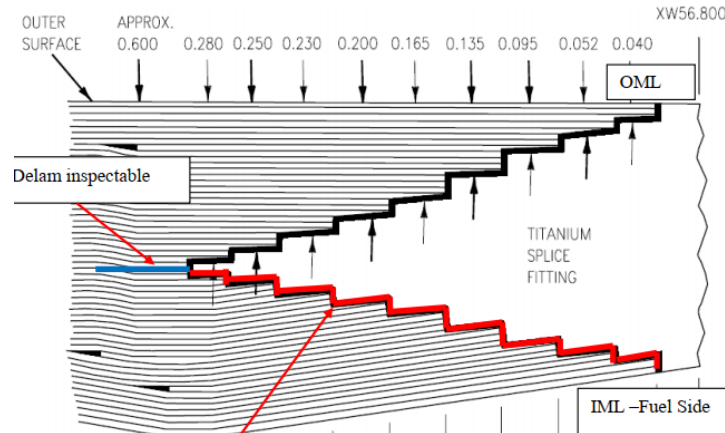
Figure 11 Step Lap Joint Overview

The primary goal of this test is to better understand the impact of disbonds on the structural integrity of the F/A-18 inner wing and understand the behaviour of the disbond under repeated static loads. This test will ultimately provide essential measured data to support development and improvement of the analytical tools for analyzing in-service fleet disbond(s). This data should ease the development of a less conservative and more flexible analysis methodology.

The test article will be installed inverted onto a test reaction structure. Three contour boards will be installed and two jacks per contour board will apply loads. A precise assembly has been designed and manufactured to replicate the wing attachment lugs found on the actual aircraft fuselage centre barrel. A challenge was to design parts within the envelope of the actual fuselage bulkheads which must withstand loads higher than OEM ultimate loads, while keeping cost and machining complexity under control. This test article interface is currently under rework at L3 MAS using similar procedures used on actual fuselage centre barrels, to ensure a good fit with the test article.
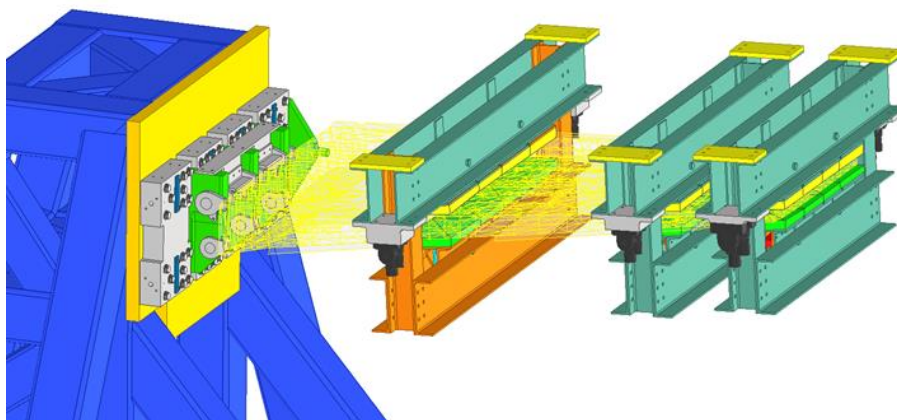
Figure 12 Load Introduction Interfaces

The test article is exhaustively instrumented to quantify the impact of a disbond on the load distribution (panel and internal structure). Both upper and lower panels are equipped with optical fibres to measure the strains between the main carry through bulkheads. Over 258 strain gauges were strategically installed on the composite laminate and metallic structures. Digital Image Correlation will also be used to evaluate the strains on the upper and lower skin panels. Displacements will also be measured.

The test article will be subject to four (4) phases. Phase A is a calibration step where the expected strains (FEM) will be compared to actual strains. Deviation will be investigated and adjustment will be made to address any issue. Phase B will apply, once, the peak and valley loads of three (3) load cases followed by a thorough inspection of the SLJ. Upon inspection, two (2) blocks of 1,000 occurrences of the peak and valley loads for those same three (3) load cases will be applied. A thorough inspection of the SLJ will be conducted between each block. Phase C and D will consist in repeating Phase B with scaled loads (1.05 and 1.10 overall factor). The last phase, Phase E, will use the same three (3) load cases, but scaled to the RST load level (1.2 DLL x Environmental Factor).

There is a provision to induce artificial damage that should not or only minor growth occur. The scope of work and method for inducing such damage is yet to be determined.

All testing will be carried out at the Structural Integrity Laboratory, Building M-14, NRC Aerospace Research Centre, Montreal Road Campus in Ottawa, Ontario, Canada. The testing will start in January 2022 with planned completion by April 2022.

3.0 AIRCRAFT STRUCTURAL INTEGRITY PROGRAM AND FLEET MANAGEMENT

3.1 CF-188 Aircraft Structural Integrity Program (ASIP) and Aircraft Life Extension (ALEX) Program

L3 Technologies MAS, Inc., a subsidiary of L3Harris Technologies, Inc. (L3 MAS)

L3 Technologies MAS, Inc., a subsidiary of L3Harris Technologies, Inc. (L3 MAS), is among Canada's leading In-Service Support (ISS) integrators, offering military and commercial customers a full range of modifications and sustainment solutions, in support of their aircraft and ship fleets. L3 MAS employs over a thousand people in its main facility in Mirabel, Quebec and in other operating centers throughout Canada (Bagotville, Cold Lake, Halifax, Shearwater, Comox, Pat Bay, Greenwood, Gatineau, Ottawa, Toronto, Trenton and Petawawa).

Since 1986, L3 MAS has conducted in-service support of the Royal Canadian Air Force (RCAF) CF-188 Hornet (Boeing F/A-18) fleet as part of System Engineering Support Contract (SESC). This contract includes the conduct of all aspects of the Aircraft Structural Integrity Program (ASIP) and of related depot level structural maintenance. L3 MAS also fulfills a similar role in support of the CT114 (Canadair CL-41) Tutor aircraft, a fleet that the RCAF currently employ for their Snowbirds aerobatic team and the CC150 Polaris aircraft (Airbus A310). As a key partner to Lockheed Martin in the Maritime Helicopter Program (MHP), L3 MAS also performs ASIP functions on the CH148 (Sikorsky S92) helicopter. L3 MAS also provide engineering services to international F/A-18 operators such as the US Navy, armasuisse and Finnish Air Force.

L3 MAS conducts a full-fledged ASIP program on the CF-188 fleet on behalf of the RCAF. Above and beyond usage and structural condition monitoring activities mandated by MIL-STD-1530, the program has effectively extended the life of the aircraft by approximately 50% via the life extension program (ALEX). The fatigue life of the airframe is managed primarily via the Fatigue Life Expanded Index (FLEI) (computed at the wing root) as part of the Individual Aircraft Tracking (IAT) program. Other areas on the airframe are certified with higher scatter factors to account for other load influences that are not tracked by the wing root index and/or dynamic loading. The so-called Tracking Factor is embedded in the lifing in order to obtain a similar level of safety for all areas of the aircraft. Landing gear components are managed via manoeuvre counts (essentially landings and retraction cycles) and flight control surfaces are managed by component flight hours (CFH).

In late 2019, the RCAF decided to cancel the so-called ELE (Estimated Life Expectancy) Extension Program. The ELE remains 2032 but the introduction of the Interim Fighter Capability Program (IFCP), 18 jets acquired from the RAAF and the expected introduction of the Future

Fighter Capability Program (FFCP) as early as 2025, will enable the RCAF and L3 MAS to manage the fleet while maintaining the FLEI limit at 1.00 as opposed to 1.08 or 1.04 previously. This will require much reduced Non-Recurring Engineering Effort (NRE) but increased fleet management efforts through traditional FLEI management (recommendation of mission mix and FLEI increments to operators) but also through exchanges between squadrons and selective and temporary storage of some of the over-utilized assets until 2026, at which time some of the assets start to be retired.

The IFCP project has led to a substantial effort by the RCAF and L3 MAS in determining the proper fatigue life management approach for these jets acquired from the RAAF. The RCAF and RAAF have collaborated under IFOSTP and have shared some of the life extension solutions developed by L3 MAS over the years, primarily for the center fuselage and inner wings. Despite this, their management philosophies are different and as a result, currently, the IFCP aircraft are limited both in FLEI and in Airframe Hours (AFH). For the majority of the assets that have been purchased, the AFH limit (6,600 FH) will expire too early, before ELE. A fairly limited scope of on-aircraft work is being executed at import, on top of the so-called LOTEX (Life of Type Extension) scope of work prescribed by the RAAF, in order to increase the limits slightly (by 5% - 6%) where practical but a more substantial effort will be needed in the years to come.

3.1.1 FLIGHT CONTROL SURFACES LIFE EXTENSION

As previously reported in previous ICAF cycles, the extension of the life of the Flight Control Surfaces (FCS) is one of the last major efforts required to support the extension of the ELE to 2032. The FCSs are managed in CFH as mentioned above, so maintaining the target FLEI at 1.00 does not benefit them directly. The RCAF had previously adopted an interim position to use the OEM-recommended inspections at 6000 CFH which provides an extension to 7000 CFH; however, even this effort is not adequate to meet RCAF fleet requirements. Supporting the fleet until 2032, with due consideration for non-repairable defects (primarily due to environmental induced defects on honeycomb core and/or bonded joints), has led to a need to certify FCSs to 8,000 or 9000 CFH depending on the inventory at hand.

The certification strategy is primarily based on full-scale component testing of the Horizontal Stabilator, the aileron, the inboard leading edge flap and the trailing edge flap. L3 MAS and the NRC, the test agency, are working in close collaboration on these programs. Testing of the Horizontal Stabilator and of the aileron were completed as of the last reporting cycle in 2019. Further details are provided below on the other FCSs at stake:

Trailing Edge Flap Tests (TEF)
The Trailing Edge Flap (TEF) attach hinges do not meet the ELE target of 8,000 CFH. Due to the urgency of certifying the outboard hinge, it was decided to set up a dedicated test for that purpose alone. The outboard hinges have been replaced and have two hot spots that have been subjected to

modifications shortly after the replacement: An oversized and cold worked lug hole and a blended and shot peen surface area near the lug. Results of this test have only allowed a moderate extension of the life of the hinge and some hinges will fall short of the 8,000 CFH target if they were replaced and/or were modified too early. The situation is currently being assessed at the asset management level to see if component swaps will be sufficient to meet the ELE.

The inboard hinge also has two known hot spots, one of which was found cracked in-service. This tends to suggest that previous certification tests were insufficient. The strategy to bridge the gap from the current 7,000 CFH (OEM/USN) limit to 8,000 CFH is currently in discussion with the RCAF while inspections are also being deployed in the fleet in the meantime.

Inboard Leading Edge Flap (ILEF)
The ILEF fatigue life is limited by the lower of the overall component limit, currently set at 8,000 CFH or the life of the transmission lugs following a modification (blend and shot peen the root radius with dedicated robotic suite). The main objective of the test was to test the transmission lugs, it was successfully completed in 2020, including the test interpretation effort and has enabled an extension of the associated limit from which the fleet will benefit.

3.1.2   OUTER WING MAINTENANCE INDUCED DAMAGE (MID) TEST

MID has been reported on both the RAAF and RCAF F/A-18 fleets at the Lower and Upper surfaces of the outer wing forward spar at the root of the Outboard Leading Edge Flap (OLEF) transmission attach lugs. These appear to have been induced by sharp instruments used to cut the sealant above these lugs under the seals, likely from in-service maintenance (see Figure 13). The MID location also coincide with the peak stress location on these lugs (see Figure 14). This leads to initiation and apparently fast propagation of cracks severing several lugs before they were detected.
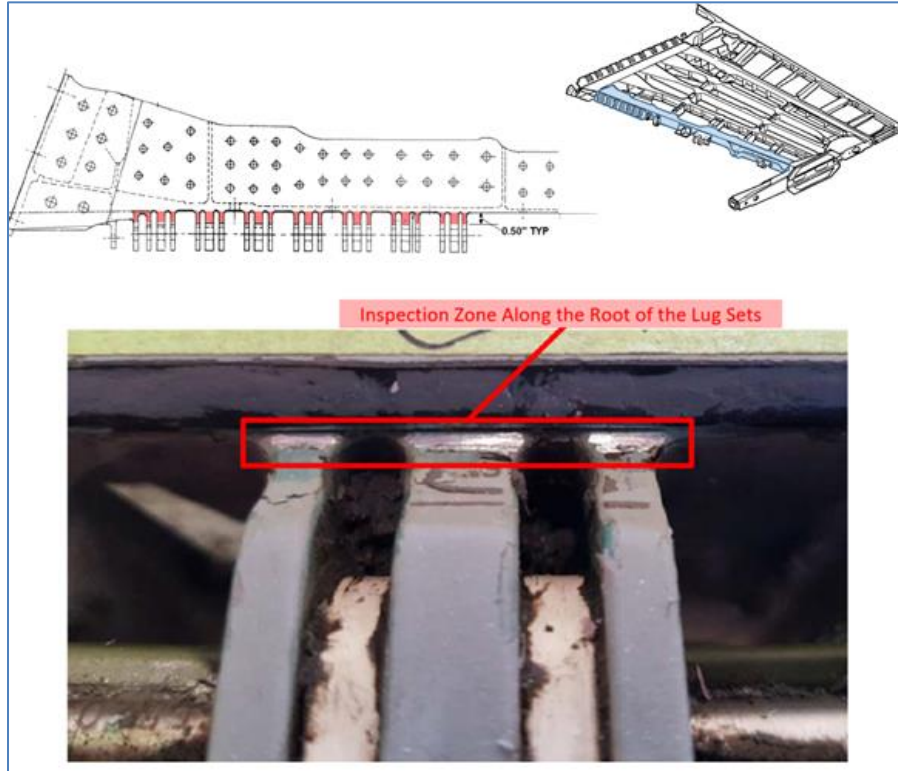
Figure 13 OW Forward Spar MID Location
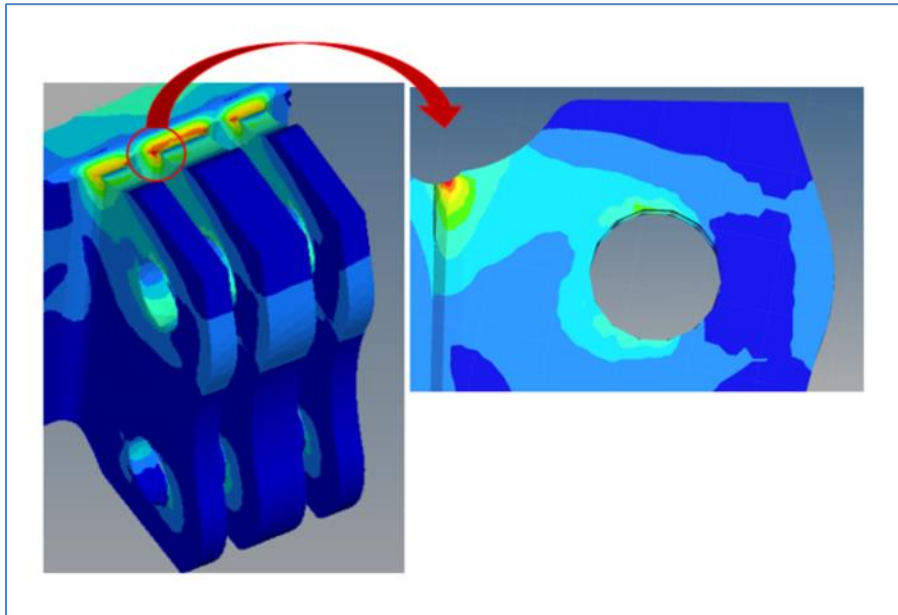
Figure 14 OW Forward Spar peak Stress Location

The repair concept (originally developed by the RAAF) was not considered full life and only substantiated analytically in crack growth leading to fairly small post repair inspection intervals

(see Figure 15). For example, the re-inspection interval was 227 hrs for a blend of 0.040" deep with a radius 0.125''. Since the RCAF are expecting to fly their outer wings longer than the RAAF, a longer post repair life was desired. Since the repair concept was already developed with a portable milling fixture, the RCAF decided to adapt this repair solution but at the same time ensure that a post repair Crack Initiation (CI) life can be accounted for, not only Crack Growth (CG). This was ensured by performing a confidence cut after the damage is removed. In addition, to repair deep damage, a revised deeper repair scenario was developed using a wider blend radius. This deeper blend will be accomplished using a numerical controlled milling fixture.

Figure 15 Light Repair Blend

The certification of the light blend repair version (covering the majority of wings) is to be covered by component testing at NRC, Ottawa under FT390 (see Section 2.2). The deeper blend will therefore be "pegged" on the test results using ratio of stresses from FEA.

The test article includes an Outboard Leading Edge Flap mounted on an OW with four jacks applying maneuver loads. After a loads influence review if was found that wing bending loads had negligible influence so only OLEF loads are applied. Then each lug was instrumented adjacent to the blend area (see Figure 16). The test is on-going.
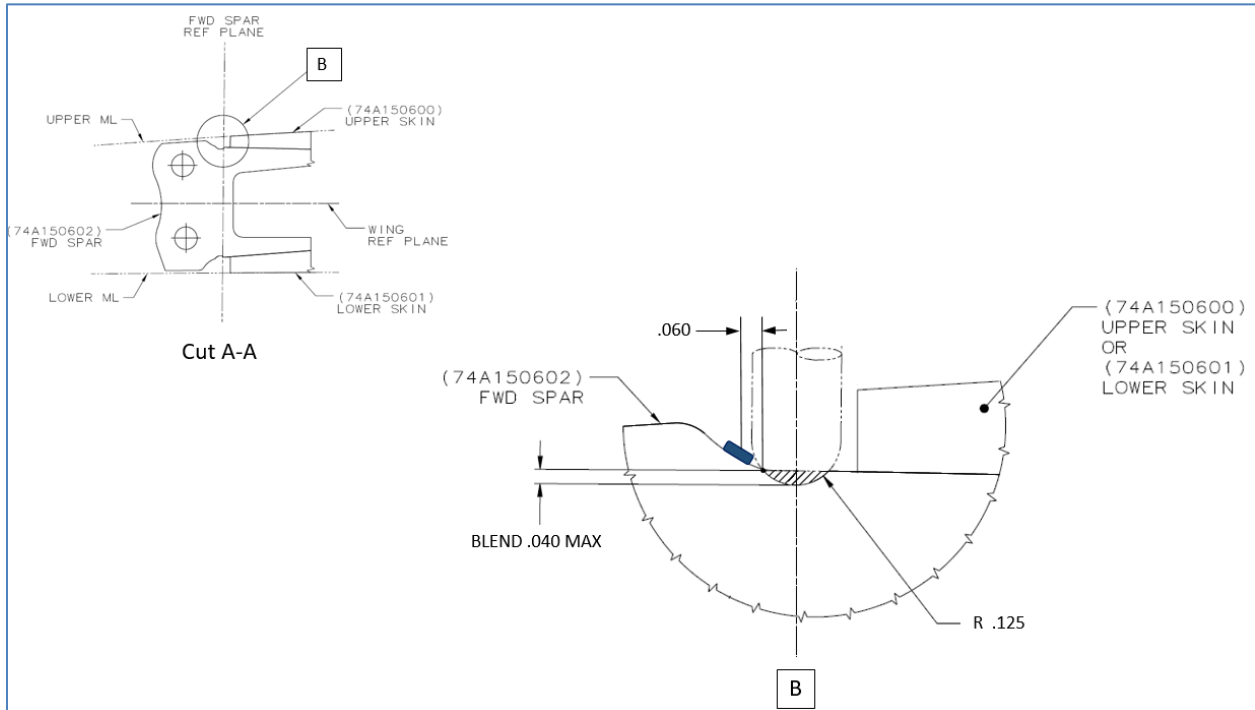
Figure 16 Strain Gauge Location

3.1.3 COUPON TESTING FOR CG LOCATIONS UNDER COMPRESSIVE LOADINGS

Several life limited locations on the CF-188 fleet fuselage parts are subjected to compressive loading, i.e. compressive loading for +ve Nz excursions and low-moderate tensile loading for –ve Nz excursions. The majority of the problematic (life limited) locations are at fastener holes but a few are also at fillet radii locations. Given the limitation of the existing Crack Growth (CG) software to adequately model CG behavior under a compressively dominated spectrum, a new methodology with calibrated data will be developed using coupon testing. A collaborative program with NRC and the RCAF is proposed and will be based on improving the crack growth prediction using standard software by modifying the material data to allow propagation in the low stress amplitude. While preliminary testing have shown promising results, further testing/validation is required before being able to use this approach for certification purposes.

3.2 CT-114 (Tutor) Aircraft Structural Integrity Program (ASIP)

L3 Technologies MAS, Inc., a subsidiary of L3Harris Technologies, Inc. (L3 MAS)

MAS conducts a full-fledged ASIP program on the CT-114 Tutor fleet on behalf of the RCAF. Aircraft usage monitoring is achieved by collecting, evaluating and processing the Operational Loads Monitoring (OLM) system data. Periodically, collected aircraft usage data is validated and

accumulated fatigue damage is calculated for major aircraft components. In addition, remaining life for every major aircraft component is calculated based on predicted aircraft usage by using the software tool GIFTS. The monitoring program findings and L3 MAS recommendations are reported to DND on a monthly basis.

L3 MAS was mandated to extend the service life of the Tutor fleet to 2030. This resulted in the review of teardown inspection results, structural modifications, identification and monitoring of SSI requiring inspection/rework, electrical / mechanical systems obsolescence, fabrication of components (mainly FCS) and the development of a fleet strategy to manage the rotation of service aircraft with those in storage in order to meet the new planned retirement date.

Figure 17 CT-114 Tutor (Snowbird, http://rcaf-arc-images.forces.gc.ca/gallery/caf/detail/?filename=CX03-2017-0135-08&assetId=58965)

3.3 CH-148 Maritime Helicopter Aircraft Structural Integrity Program (ASIP)

L3 Technologies MAS, Inc., a subsidiary of L3Harris Technologies, Inc. (L3 MAS)

As part of the Maritime Helicopter Program, L3 MAS is mandated to conduct an ASIP program on the S-92, designated as CH-148 by the RCAF. Usage monitoring is enabled via the S-92 Health and Usage Monitoring System (HUMS). The HUMS has the capability to recognize regimes/manoeuvres via recorded flight parameters and sensor data. This data is processed by the Usage Comparison and Reporting Tool (UCART) that computes fatigue damage rates at selected locations for each individual aircraft and compares them to the design spectrum according to the requirements of MIL-STD-1530.

Since 2019, algorithms for fatigue damage rate derivation in UCART from the HUMS regime and event data and have been corrected for improved accuracy. Also, existing control points, at which fatigue accumulation is being computed and compared to the Baseline Operational Spectrum (BOS) have been changed and others have been added for better coverage. Filtering of the captured regime data has been implemented to alleviate the excessive triggering of certain manoeuvres, within the recognition software, when aircraft is operating close to the defined thresholds. This change results in more realistic characterization of the usage.

The other major component of the CH-148 ASIP Program is the Structurally Significant Item (SSI) database. The SSI database records all the relevant information about each SSI, also known as Primary Structural Element (PSE), from the design phase and into the in-service phase in order to enable ASIP analysts to monitor structural defects and, when needed, recommend changes to the maintenance program or modifications to the helicopter.

Figure 18 CH-148 Cyclone helicopter (http://rcaf-arc-images.forces.gc.ca/gallery/caf/detail/?filename=PM06-0001&assetId=8337)

3.4 CC-150 Polaris Fleet In-Service Support and Fleet Management

L3 Technologies MAS, Inc., a subsidiary of L3Harris Technologies, Inc. (L3 MAS)

As part of the Polaris Program, L3 MAS is mandated to provide in-service support for the operations of the five CC-150 Polaris aircraft (Airbus A310-304) of the Department of National Defence's (DND). L3 MAS develops and maintains A310 maintenance schedules to satisfy 180 minutes Extended range Twin-engine Operations (ETOPS) and CC150 specific modifications. L3

MAS also provides engineering support to satisfy Canadian Forces operational requirements and the configuration control of the CC-150 Polaris (A310 Airbus) fleet, as well as Reliability monitoring based on Airworthiness Manual Advisory AMA 571.101/1 to monitor the effectiveness of the CC150 maintenance program.

Figure 19 CC-150 Polaris in tanker configuration ([Photo Detail - IS2012-2003-150 Canadian Forces Imagery Gallery](#))

3.5 Airframe Digital Twin (ADT) Technology Development and Demonstration

Min Liao, Guillaume Renaud, Yan Bombardier, Jean-Rene Poulin, Gang QI, Gang Li, NRC Aerospace

With the support of the Department of National Defence (DND) of Canada, the National Research Council of Canada (NRC) has reviewed and assessed the Airframe Digital Twin (ADT) framework being developed by the United States Air Force (USAF). The goal is to investigate the adaptability and potential application of the ADT for reducing maintenance cost and to maximize availability of existing and future fleets of the Royal Canadian Air Force (RCAF) [1]. The ADT framework is based on a probabilistic and prognostic Individual Aircraft Tracking (IAT) approach, which intends to improve the current IAT program by quantifying and updating the uncertainties of some parameters in airframe fatigue life assessment. The work performed to date includes [1]:

1) A review and evaluation of the digital twin and digital thread concepts, especially the USAF ADT framework, methods/tool;

2) A brief survey of structural lifing methods and IAT systems for selected RCAF aircraft, and a feasibility and adaptability study to apply the ADT to RCAF aircraft;

3) Development of a NRC ADT framework (Figure 20) and in-house algorithms including current load, crack growth and probability of failure (POF) prediction, crack size distribution updating with sensor and NDI results (Figure 21), and future loads and POF forecasts.

4) ADT technology demonstration using a CF-188 full-scale component certification test (Figure 22), and comparison with the existing CF-188 lifing method.
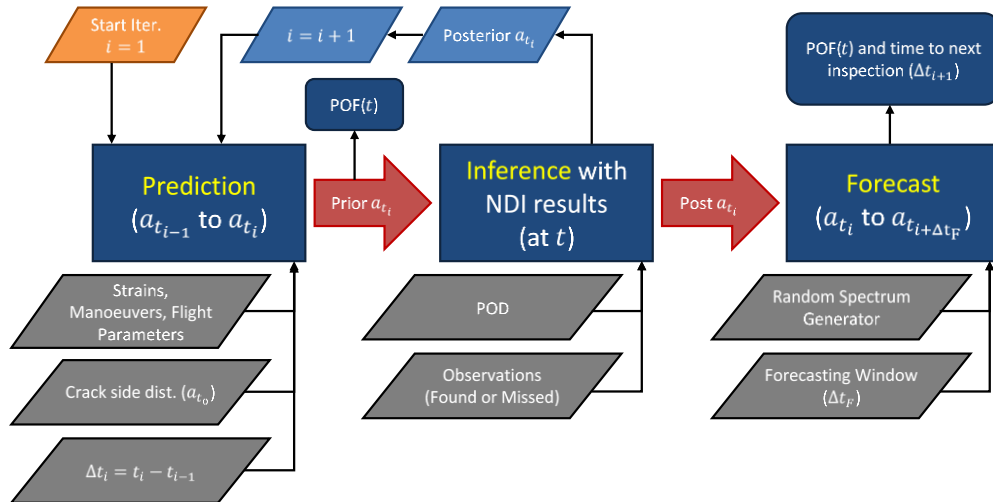
Figure 20 NRC ADT Framework 3-Phase Concept: a) Prediction is used to estimate crack size distribution at inspection time (current time) b) Inference fused the expected crack size distribution obtained from the prediction with the inspection results, and c) Forecast is used to estimate the future crack size distribution and the probability of failure (POF) as a function of time.
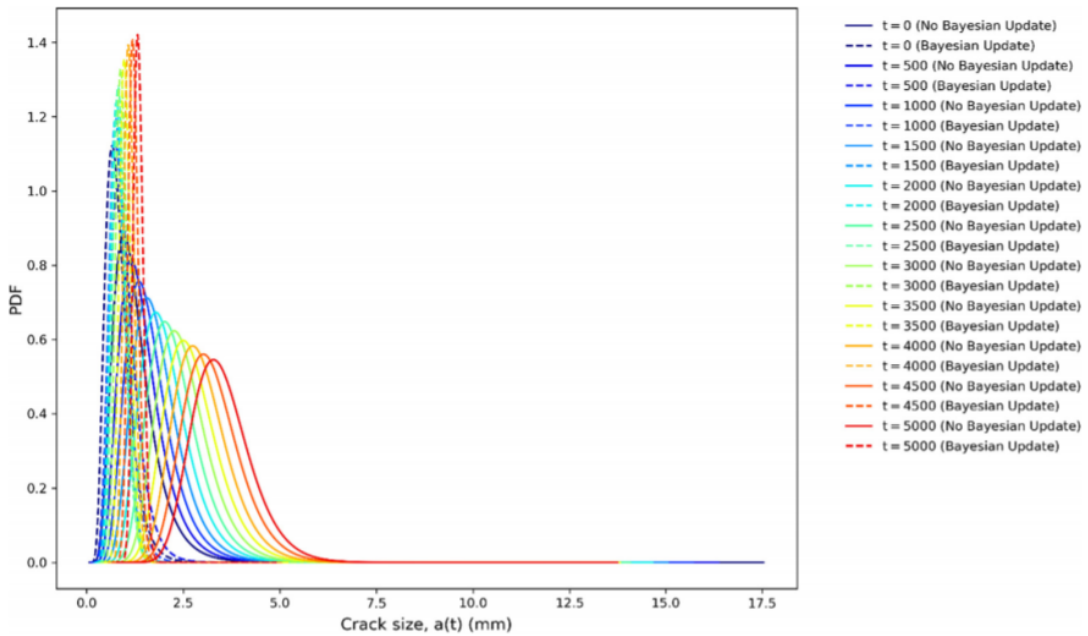
Figure 21 Crack size distributions with and without Bayesian updating, for 11 consecutive inspections with no-crack findings, starting from an initial crack size distribution with a rogue flaw assumption.
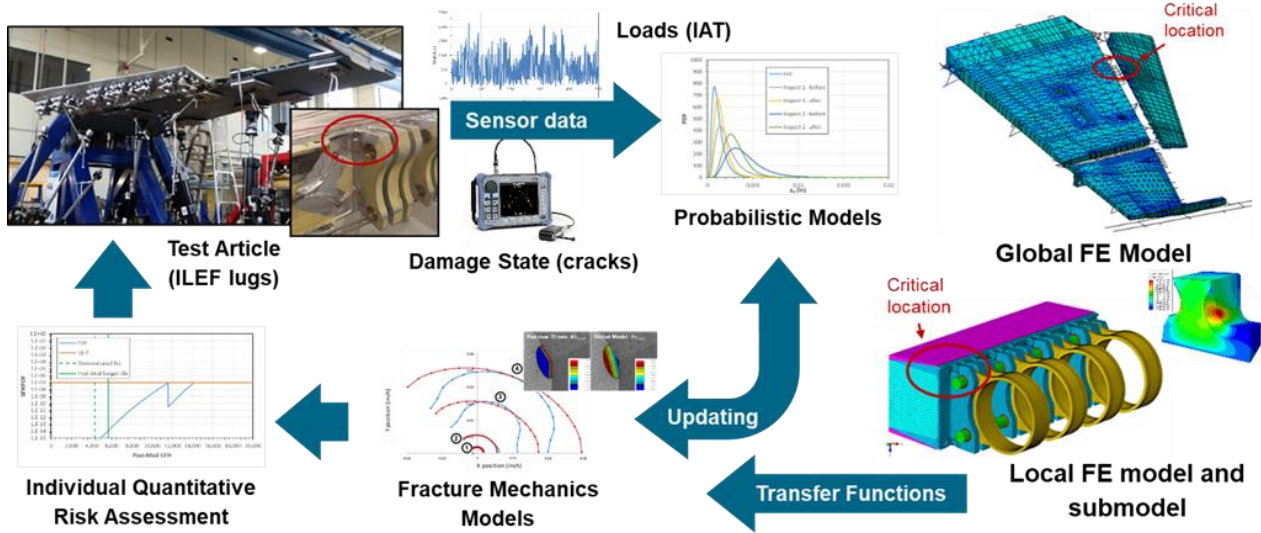
Figure 22 ADT framework demonstration using the CF-188 ILEF component test.

In summary, the NRC review and assessment show that the emerging ADT concept and framework can be adapted to support RCAF fleets that are managed using IAT-based programs. The NRC models and tools are developed with more simplicity, flexibility and efficiency that can be

implemented for RCAF fleets. Short-term benefits are demonstrated on the NRC developed ADT technology:

- first, it allows for improving the IAT system and data with quantification of variability and correlation of IAT accuracy with structural probability of failure;
- second, the high-fidelity FE model, crack growth model and Bayesian updating with all NDI inspection results improves fatigue life estimation for structural maintenance and life extension programs.

Considering the long term, a significant return on investment could be possible, with benefits that include optimal maintenance, reduced total ownership costs and increased fleet availability. Based on the ADT review and technology demonstration, NRC developed a short and long term roadmaps on ADT in support of the RCAF strategic sustainment program.

3.5.1 REFERENCES

[1]   Liao M, Renaud G, Bombardier Y. Airframe digital twin technology adaptability assessment and technology demonstration. Engineering Fracture Mechanics. 2020 Feb 15; 225:106793.

4.0 FATIGUE LIFE ASSESSMENT AND ENHANCEMENT TECHNOLOGIES

4.1 F-18 Aircraft International Support

L3 Technologies MAS, Inc., a subsidiary of L3Harris Technologies, Inc. (L3 MAS)

Over the years, L3 MAS has performed several fatigue life assessments and/or development of modifications (and inspections) for other F/A-18 operators, namely the RAAF, United Sates Navy (USN), armasuisse and the Finnish Air Force. The locations addressed via these efforts are often the same or similar in terms of configuration to those covered in the CF-188 ALEX program. The other key reason why these operators have come to L3 MAS for assistance is the unique capability that the company has developed for fatigue spectra and loads development and in-situ robotic applications, namely machining and shot peening, as previously reported.

4.1.1 LOADS DEVELOPMENT AND STRUCTURAL LIFE ASSESSMENT OF F-18 AIRCRAFT COMPONENT

The Finnish Air Force approached L3 MAS for one such location where the Finnish Air Force F-18 (FN-18) had their configuration redesigned by the original equipment manufacturer (OEM). L3 MAS was mandated to demonstrate the fatigue life of this part for the FN-18 typical usage. This resulted in the derivation of the average fleet aircraft fatigue spectra using the L3 MAS in house software Enhanced Load Software Application (ELSA) along with in house Matlab scripts. The resulting manoeuver + dynamics spectra contained about 700 000 points in the sky (PITS) after down sampling for fatigue crack initiation analysis. This represents approx. 130 flight hours for the average fleet aircraft.

The regression for the area of interest was obtained from the strain gauge installed during the L3 MAS center fuselage fatigue test. However, this strain gauge was installed on the older configuration. Using the Finite Element Model (FEM) created for this area, the strain gauge equation was corrected to the redesigned part configuration. This regression, the previously derived spectra and material properties were passed through another L3 in house software to obtain the estimated crack initiation life of the part. Based on the previous, the aircraft structural integrity was demonstrated for the full life of the aircraft in crack initiation alone. Thus, no further action was recommended to the client.

4.2 Fatigue Crack Growth under Highly-Compressive Spectrum Loading

Guillaume Renaud, Jean-Rene Poulin, Yan Bombardier, NRC Aerospace

Some of the life limiting items (LLI) of the CF-188 have characteristics that make their certification challenging to reach revised life targets with existing models and data. The National Research Council of Canada (NRC) was tasked by the Canadian Department of National Defence (DND) to investigate methods for increasing the demonstrated life of some of these problematic LLIs. Potential approaches to do so include: leveraging additional existing models and data, developing new test data, and/or developing alternative analysis approaches.

The first problematic LLIs investigated by NRC are subject to highly-compressive variable amplitude spectrum loading. Compared with historical testing and in-service data, the current models predict excessively large fatigue crack growth lives and cannot be used for fleet maintenance.

AFGROW simulations that were conducted to replicate previous tests of aluminium 7050-T7451 coupons with fastener holes [2] confirmed this discrepancy. Furthermore, only marginal improvements of the predicted fatigue crack growth lives were obtained when effects such as the tensile residual stresses at the hole and the hole-filling effect were included in the models. After performing a model calibration study, it was hypothesized that the discrepancy between the analytical and experimental results was mainly due to the poor representation of the near-threshold region of the fatigue crack growth curves currently used for aluminium 7050-T7451. Indeed, it is shown in the literature [3][4][5] that roughness-induced crack closure plays a significant role in the fatigue crack growth behaviour of this alloy. The contribution of this effect is such that the measured fatigue crack growth threshold can be shifted towards larger stress intensity factor ranges, which leads to underestimated crack growth rates in this region. In a context of highly-compressive spectrum loads, where typical cycles consist of high compressive loads and low tensile stresses, an accurate representation of the near-threshold fatigue crack growth rates is paramount for accurate life predictions.

New 7050-T7451 coupons were manufactured with the intent to generate high-quality fatigue crack growth curves for the considered spectra, while focussing solely on the material aspects of the problem. The objective was to develop a material model that could reasonably predict fatigue crack growth lives under highly-compressive as well as regular tension-dominated spectra. To date, six M(T) coupons have been tested. Three tests were conducted under a standard wing root bending spectrum (FT55), and three were tested under the inverted version of this spectrum (inverted FT55). Multiple candidate AFGROW models were built by combining "closure-free" data from the literature with existing CG90, AFGROW and NASGRO models.

The life prediction obtained with AFGROW using current material data is compared with one of the new models in Figure 23. The lives predicted by the current model are conservative for the standard spectrum but non-conservative for the highly-compressive spectrum. The lives obtained with the new model are closer to the test data and are both conservative.
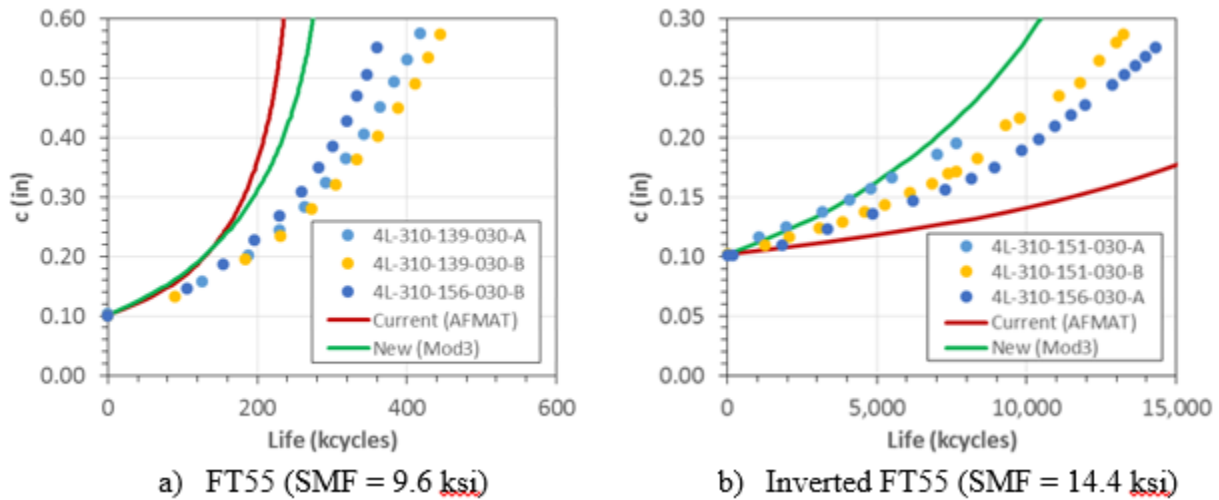
**Figure 23 Experimental fatigue crack growth curves compared with
current and new model predictions**

Work performed to date confirms that a closure-free representation of the near-threshold fatigue crack growth rates is a promising approach to better predict the lives of LLIs subjected to highly-compressive spectra. Current work is focussing on validating the applicability of the developed material model for problems that are more representative of the LLIs under investigation. To this end, fatigue crack growth tests for an interference-fit fastener hole are currently being prepared to be conducted under tensile-dominated and highly-compressive loading spectra. These additional data will help select and refine a new material model, as well as validate fastener effect modelling approaches. It is believed that the model being developed will be helpful for managing the CF-188 fleet for some of the problematic LLIs that are currently difficult to certify.

4.2.1   **REFERENCES**

[2]   Tessier, S., "Guidelines for Using CI89 and CG90 Tools with Highly Compressive Loading", GAL-318-0263 Rev. B, L3 MAS, June 2010.

[3]   Newman, J.C., Yamada, Y., and Newman, J.A., "Crack-Closure Behaviour of 7050 Aluminum Alloy near Threshold Conditions for Wide Range in Load Ratios and Constant Kmax Tests", Journal of ASTM International, Vol. 7, No. 4, 2010.

[4]   Walker, K.F. and Barter, S.A., "The Critical Importance of Correctly Characterising Fatigue Crack Growth Rates in the Threshold Regime", 26th ICAF Symposium, Montréal, 1-3 June 2011.

[5]   Walker, K.F., "Roughness-induced crack closure in the threshold region for high strength aircraft structural alloys", RMIT University, 2015.

4.3 Numerical Assessment of Stress-Intensity Factor of a Corner Crack at a Cold-Expanded Hole

Gang Li, NRC Aerospace

The effect of specific loading histories on the stress intensity factor (SIF) of a 0.05" radius corner crack at a cold-expanded hole with original radius of 0.25" was studied numerically. As shown in Figure 24, the planar corner crack was located on the transverse symmetric plane of a 0.25" thick 2024-T3 aluminium alloy plate to represent a typical Mode I crack found widely in aircraft structures. The plate dimensions used can represent larger plates for the study because the residual stress condition induced by hole cold expansion (Cx) process was found to be unaffected by the use of larger dimensions. The model was compared with an analytical solution obtained for Mode I SIF in linear elastic fracture mechanics (LEFM) conditions without residual stresses. Good agreement in the SIF values was obtained between the numerical and analytical solutions, within a 5% relative difference. Then, an advanced modelling approach with multiple load cases was developed to investigate the Mode I SIF variations for a 3% cold-expanded hole subject to specific additional remote overloads. Overloads of half the yield strength and of the full yield strength were used in tension and compression, as shown in Figure 25. An elastic-plastic material model, with either an isotropic or kinematic hardening behaviour, was set in the initial load steps, and a linear elastic material behaviour was set in the final step to calculate the SIF values under remote loading. Results suggest that:

(i)   the Cx process considerably improved fatigue resistance by producing "negative" effective crack SIF values; and

(ii)   effects of tensile overloads on the cold-expanded hole could be: (a) limited for the half yield strength level, and (b) highly detrimental for the full yield strength level.
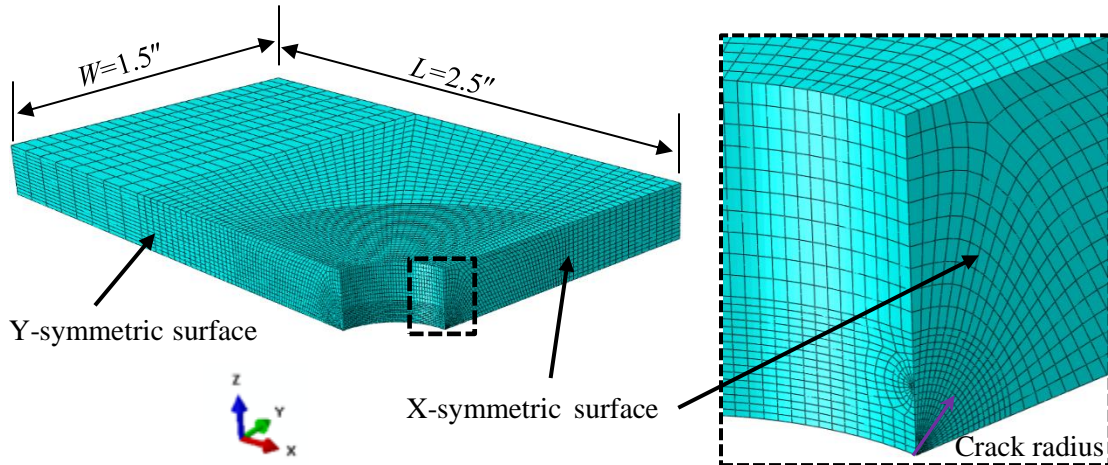
Figure 24 A quarter plate used for the numerical study of the stress-intensity factor (SIF), K_I, and the model was meshed with C3D20R solid elements.

(a) SIF affected by the residual stress (RS)   (b) SIF affected by RS and additional loading
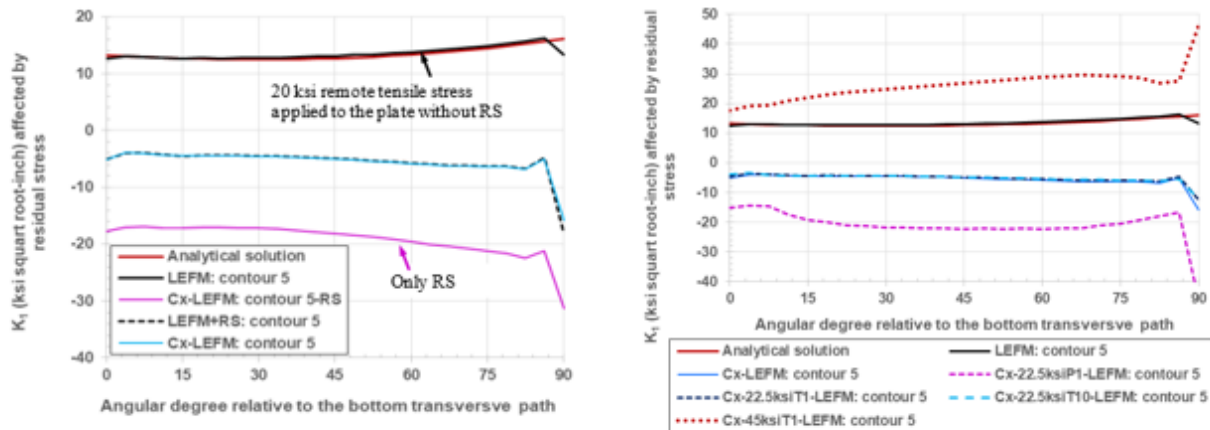
Figure 25 Comparison of the SIF variations in the isotropic hardening material behaviour: (a) with and without the RS induced by the cold expansion (Cx) process, and (b) affected by additional loading cases; where "T1", "T10", and "P1" refer to the additional loaded in tension one time, ten times, and compression one time using the relevant stress ($0.5\sigma_y = 22.5$ ksi, or $\sigma_y = 45$ ksi).

4.3.1 REFERENCES

[6]   G. Li, G. Renaud (2020), " Effect of Loading History on the Stress-Intensity Factor of a Corner Crack at a Cold-Expanded Hole", NRC Aerospace, Laboratory Technical Report, LTR-SMM-2020-0053.

4.4 Aircraft Structure Remaining Useful Life Assessment Towards Digital Twin Ecosystem

Teng Wang and Zheng Liu, UBC Intelligent Sensing, Diagnostics, and Prognostics Research Lab

Traditional health management in the aerospace industry is driven by the entity in its physical space, with little connection to its virtual space. The development of the digital twin concept makes it possible to implement the seamless convergence of physical and virtual space. A collaboration between NRC and UBC Intelligent Sensing, Diagnostics, and Prognostics Research Lab (ISDPRL) is currently investigating the fatigue life assessment towards digital twin ecosystem.

Digital twin is generated and utilized in an ecosystem, where multiple components are integrated together. ISDPRL validates the Bayesian inference-based digital twin ecosystem for aircraft structure, as shown in Figure 26. Specifically, onboard sensors and nondestructive tests provide information on the individual physical structure. The fleet database comprises predictive models, initial assumptions and prior knowledge for fatigue life assessment. Bayesian inference connects the individual physical structure and fleet database updating its counterpart digital twin structure in the cyberspace. Thus, the remaining useful life (RUL) of the physical structure can be predicted by examining its digital twin. The service station organizes the real-world activities (such as inspection, repair, and overhaul) according to the assessment results.

ISDPRL validated the above digital twin ecosystem at the coupon level with the Virkler-Hillberry data set. Figure 27 (a) shows the diagram of the tested coupon. Figure 27 (b) exhibits the duplicated holographic model. ISDPRL is currently working on validating the above digital twin ecosystem for more complicated scenarios where multiple time-varying factors are considered for remaining useful life prediction.
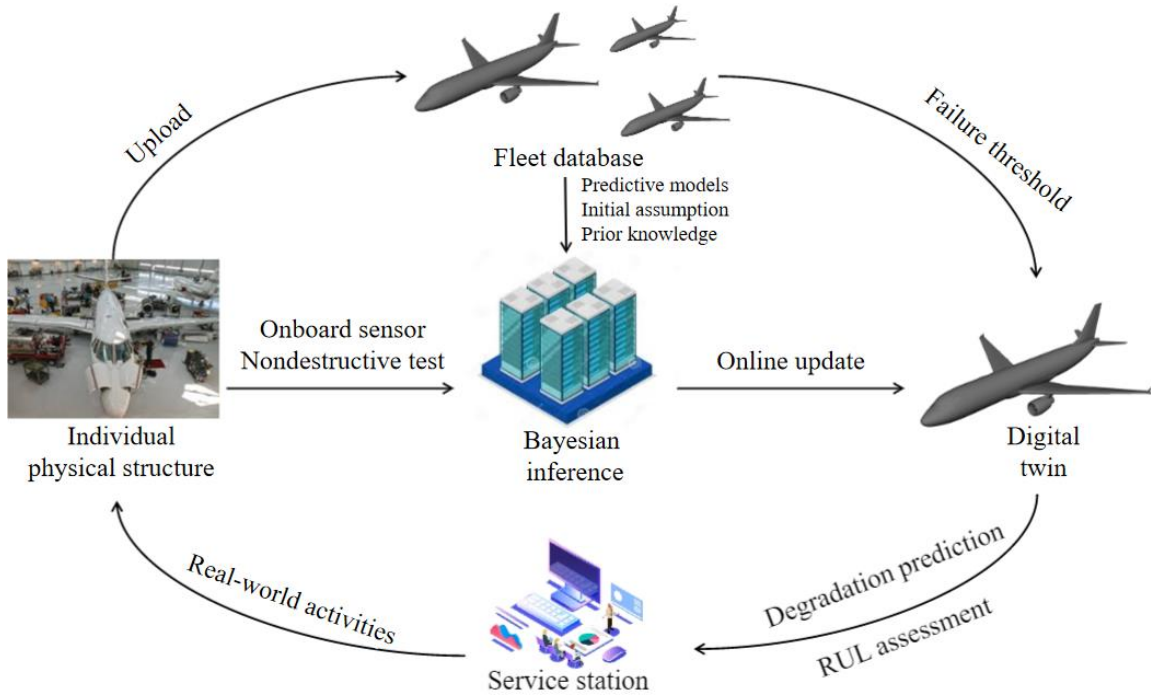
Figure 26 Digital twin ecosystem for remaining useful life assessment.
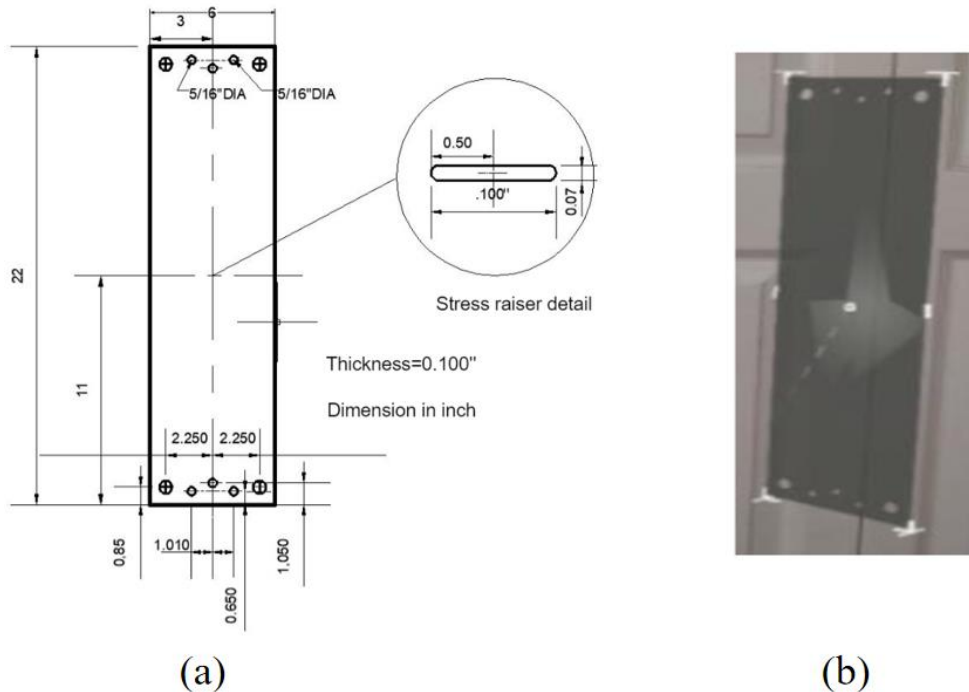
Figure 27 (a) Diagram of the tested specimen. (b) Duplicated holographic model.

4.4.1 **REFERENCES**

[7] T. Wang, Z. Liu, M. Liao, and N. Mrad, "Life prediction for aircraft structure based on Bayesian inference: towards a digital twin ecosystem." Annual Conference of the PHM Society. vol. 12, no. 1, pp. 1-8, 11/09/2020-11/13/2020, Virtual conference.

5.0 LOAD, USAGE, AND STRUCTURAL HEALTH MONITORING

5.1 CT-142 Operational Loads and Engine Monitoring System

Stephane Brunet, NRC Aerospace

The CT-142 aircraft is a military version of the De Havilland Canada DHC-8-100 used by the Royal Canadian Air Force (RCAF) for air navigation training. The current role of this aircraft differs significantly from the original commercial transport role for which the DHC-8-100 was certified. As a result, the Original Equipment Manufacturer (Bombardier, at that time) conducted an assessment of the additional fatigue damage induced on the aircraft structure due to its new role. For this purpose, the vertical acceleration data was recorded during a full calendar year on one instrumented aircraft. Subsequent data analysis enabled the quantification of fatigue damage on the CT-142 in comparison to the commercial version.

Almost two decades later, the mission profiles flown by the CT-142 aircraft have changed and the RCAF would like to re-evaluate the actual usage and its impact on the fatigue damage on the structure. The RCAF therefore mandated NRC to develop an Operational Loads Monitoring System (OLMS) to be installed on one or more of the fleet, for continuous recording of the vertical acceleration during every flight. Data processing, which would follow a similar process used until recently on the CC-115 Buffalo, would be done on a regular basis and permit an accurate evaluation of the accrued fatigue damage induced on the aircraft.

The OLMS hardware is built around an Inertia Measurement Unit (IMU), which captures linear accelerations, rate of rotations and Earth's magnetic field vector components in all three axes. The IMU output data is captured by a National Instruments standalone controller, which applies a timestamp and records the data on flash memory for later download and offline processing. A single prototype OLMS is to be installed on one aircraft for initial testing in Fall 2021. Following this, the option to instrument the remaining fleet will then be evaluated.

In parallel to the structural OLMS, the RCAF also tasked NRC to evaluate the feasibility of integrating the data collection of engine parameters required for health monitoring of the two PW120 turboprop engines. Currently, the crew collects a set of parameters manually on a paper form at one single and specific time during the flight. As this method has several drawbacks, an autonomous data collection system which would continuously record engine parameters during all flights would be desirable. Considering the customization possibilities offered by the standalone controller used for the OLMS, NRC has shown that the engine data collection feature could be added to the current OLMS system. The results of this engine monitoring feasibility study are currently under review at the RCAF.

Figure 28 CT-142 (Dash-8, http://rcaf-arc-images.forces.gc.ca/gallery/caf/detail/?filename=CX2005-0096-251a&assetId=9131)

5.2 Helicopter Load and Usage Monitoring Research in 2019-2021

Catharine. Cheung, NRC Aerospace

5.2.1 LOAD ESTIMATION AND THE USE OF MACHINE-LEARNING TECHNIQUES

Indirect methods of estimating component loads based on existing aircraft sensor data have been in development using flight data from an Australian Black Hawk (S-70-A-9) helicopter and CH-146 (Bell 412) Griffon helicopter, illustrated in Figure 29. The load and fatigue life results obtained thus far have shown tremendous potential for accurate and consistent estimates using the same methodology on both platforms. Refinements to the machine learning models are ongoing as efforts continue to explore different types of model architectures and model settings. These models and their results could all be combined in the load estimation framework to provide an ensemble of models, leveraging a number of machine learning models to result in robust and accurate estimates.

As the development of machine learning-based solutions becomes more and more common for individual aircraft tracking and digital twin objectives, preparing for future implementation of these technologies is also a focus of this work.
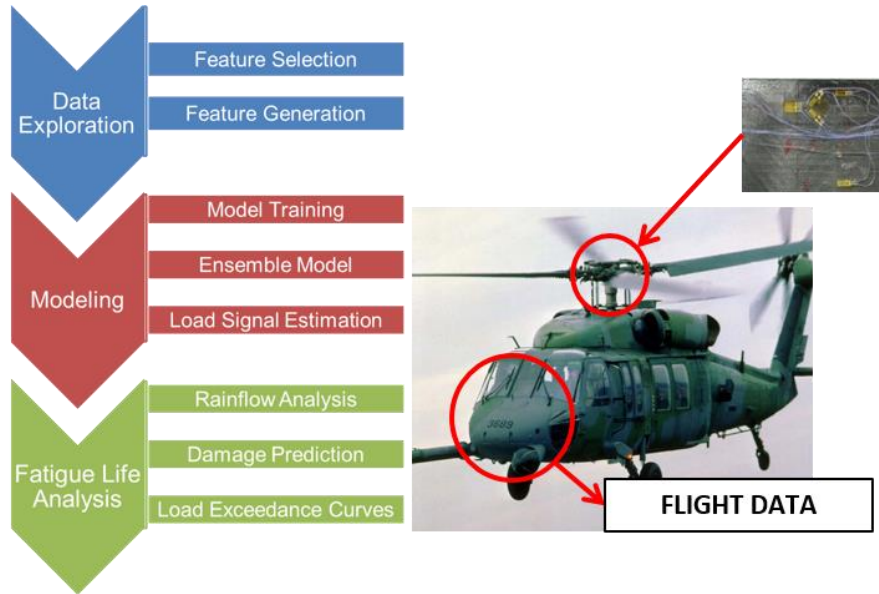
Figure 29 Illustration of load estimation approach

5.2.2   GROSS WEIGHT AND CENTRE OF GRAVITY ESTIMATION

Weight and balance activities are widely recognized and understood as important steps in the operation and maintenance of an aircraft to ensure safe and efficient flight. Figure 30 shows a typical gross weight vs centre of gravity chart. From the pilot's perspective, the operational limits and manoeuvrability of the aircraft are directly linked to the weight and balance of the aircraft. From a structural perspective, fatigue damage can vary significantly with centre of gravity (CG) position and gross weight (GW). In-flight CG and GW estimation has been pursued for many years with varying success. One of the major challenges is the lack of data to verify an estimation model, since these parameters cannot be easily measured using sensors in flight.

Efforts in this domain include a detailed review of the requirement and challenges of accurately monitoring centre of gravity and gross weight, including relevant information from flight manuals, maintenance manuals and other documentation. In addition, a survey of published work on the estimation of these values was carried out, with four main approaches identified:
   1. helicopter dynamic models;
   2. performance charts;
   3. state estimation, and
   4. machine learning methods.

An initial helicopter model for CG position and GW was generated. The intention was to utilize the available information to create an initial model that could be later expanded and enhanced with more information such as flight data parameters in the future.
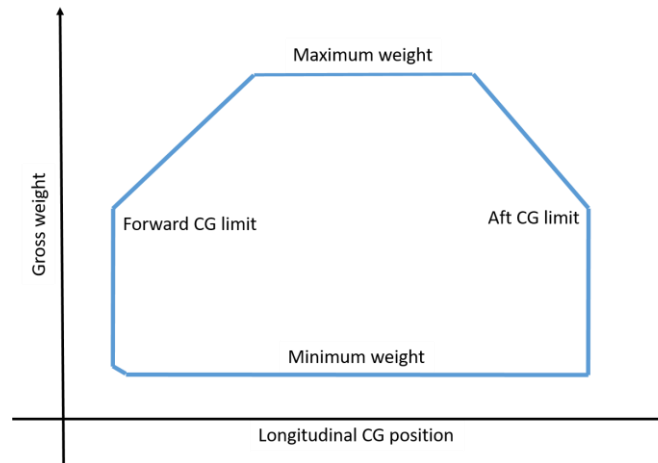
Figure 30 Typical operational envelope for gross weight and longitudinal centre of gravity position

5.2.3 ANALYSIS OF SENSOR NETWORK DATA FOR FAILURE MODELLING AND PREDICTION

The interest in data analytics and using machine learning techniques to analyse data has extended to the domain of examining and improving maintenance programs for mechanical vehicles. Equipment health monitoring has been employed for many years with hundreds, if not thousands, of sensors installed on vehicles for recording operator inputs and corresponding equipment outputs. It is hoped that useful information can be extracted from the sensor data, ideally, for preventing failure incidents, or, more modestly, for improving maintenance programs.

Efforts continue to characterize the healthy and failed/non-healthy states of various vehicle systems (e.g. diesel engine system, gas turbine system) based on data related to known failure and maintenance incidents recorded on several vehicles of the same type. Some of the machine learning tools that have been implemented include classification models, anomaly detection models, and data reduction techniques such as low-dimensional mappings as shown in Figure 31.

Similar to many failure modelling and fault identification problems, there is a clear imbalance between the majority, operational, 'healthy' data class and the minority, deteriorated, 'failed' data class. Not only are there few examples of the minority 'failed' class, there is a wide range of possible failure incidents that could be experienced, and few repeated examples of the same type of incident. For these reasons, inclusion of anomaly detection models is a clear choice because they seek to characterize the normal or 'inlier' state. An optimal system model should be able to detect new failure incidents that it has not been trained on.
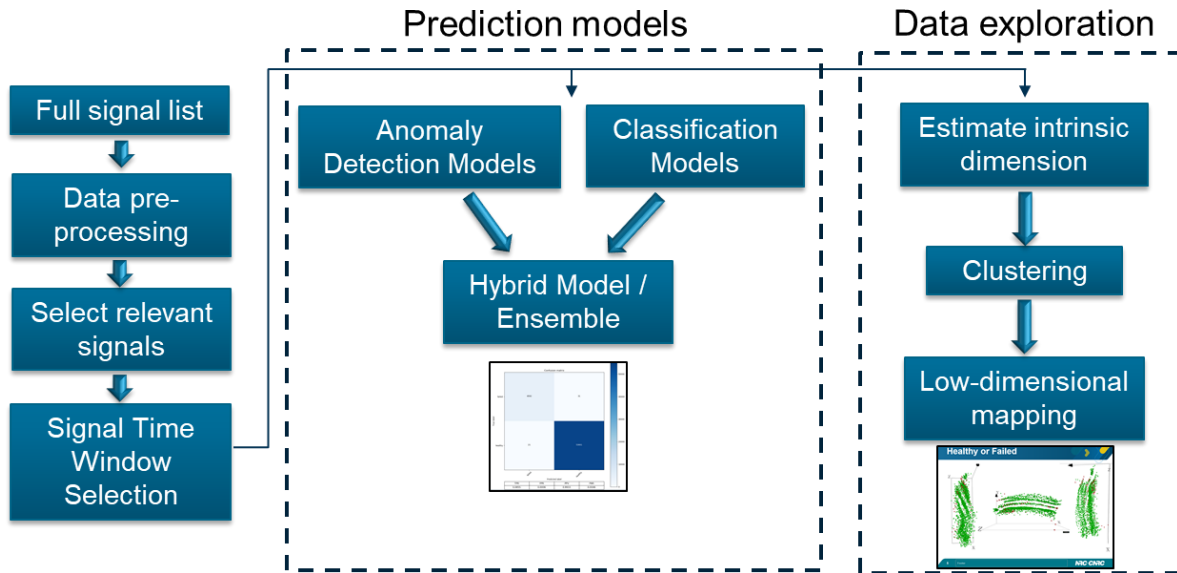
Figure 31 Analysis approach and tools

In addition, an ideal system model should be robust and flexible enough to be applicable to different vehicles of the same type, though clearly every system and vehicle are not identical. Therefore determining the appropriate data to train the system models is a very important consideration. Two strategies for selecting training data were explored in this work: a traditional approach of randomly selecting a certain percentage of data for training and leaving the rest for testing; and a more deliberate selection of data by failure incident to be used for training or testing. An assortment of classification and anomaly detection models were implemented to distinguish 'healthy' from 'failed' or 'non-healthy' system data using the two training approaches. These models were then combined into an ensemble using a decision table with promising results (Figure 32). Significant differences in the results were obtained depending on the approach to selecting training data, which would be an important consideration for similar problems in other domains.
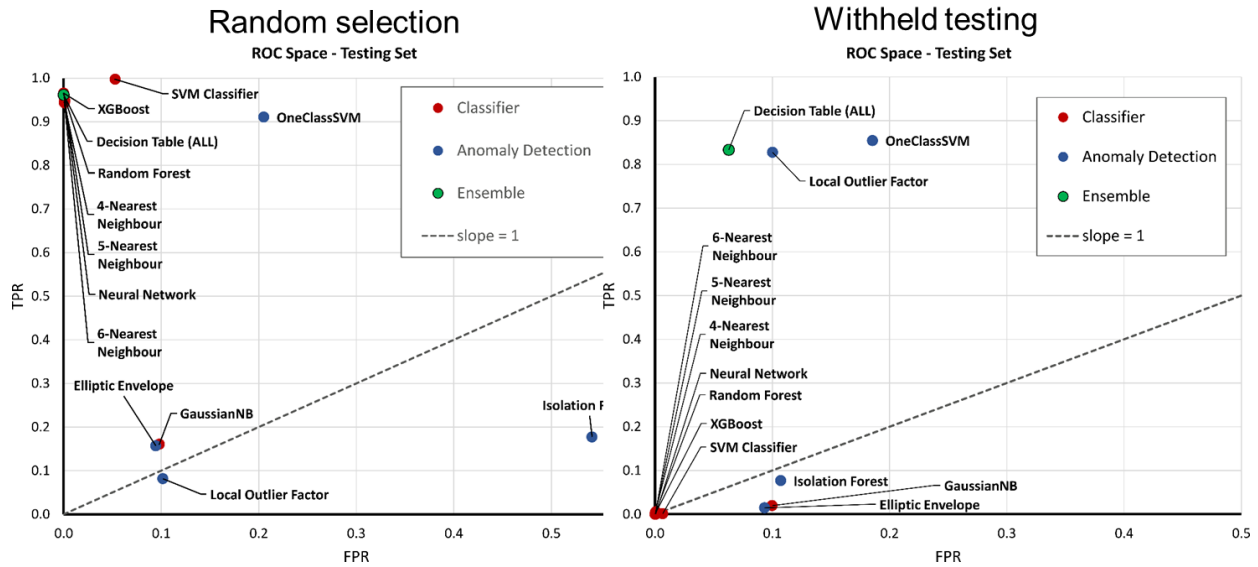
Figure 32 Classifier and anomaly detection model results in two-class problem

5.2.4 REFERENCES

[8] C. Cheung, "Load estimation and the use of data-driven/machine-learning techniques", 19th International Workshop on Holistic Structural Integrity Process (HOLSIP), Feb 2020.

[9] C. Cheung, "SHM & HUMS Research at NRC", NRC-APDC Certification by Analysis (CbA) International Workshop, Oct 2019.

[10] C. Cheung, D. To, "Monitoring gross weight and center of gravity position: A review of the challenges and current estimation approaches", Proceedings of the 76th VFS Annual Forum 2020, virtual, Oct 2020.

[11] C. Cheung, D. To, J.J. Valdés, "Failure modeling in a gas turbine system: Combining classification with anomaly detection models for two data selection strategies", Proceedings of the 2020 IEEE Symposium Series on Computational Intelligence (IEEE-SSCI), virtual, Dec 2020.

[12] S. Sehgal, C. Cheung, J.J. Valdés, "Characterizing the current state of a propulsion engine: A comparison of machine learning frameworks", CASI 64th Aeronautics Conference (AERO19), Montreal, QC, May 2019.

6.0 NON-DESTRUCTIVE EVALUATION

6.1 A Robotized Non Destructive Testing R&D

L3 Technologies MAS, Inc., a subsidiary of L3Harris Technologies, Inc. (L3 MAS)

L3 MAS is an active member of three on-going collaborative R&D initiatives with universities, colleges and industrial partners: CRIAQ (Quebec Aeronautical Industrial Research Consortium), CARIC (Consortium for Aerospace Research and Innovation in Canada) and MICA (Metrology and Inspection of Composites in Aerospace). Internal and collaborative projects that have been completed recently were in the areas of Structural Health Monitoring (SHM), shot peening, robotics and composite materials as well as software tools in support of fatigue life assessments and in-service monitoring/management, including Artificial Intelligence (AI) initiatives.

L3 MAS is currently proceeding with full scale testing of a Robotized Non Destructive Testing on control surfaces for the CF-188 and CT-114. A mobile gantry system using collaborative robots is used to acquire phased array ultrasonic data either on individual components (Figure 33) or directly on the aircraft (Figure 34). A sequencing program managing probing operations ensures that the component is correctly located in aircraft coordinates. The ultrasonic controller simultaneously acquires pulse-echo from both sides of the part as well as through transmission signals, generating a C-Scan of the component. The data is then cross-referenced to assist in determining the type of damage found and compared with nominal results.

Figure 33 Robotized Component Inspection
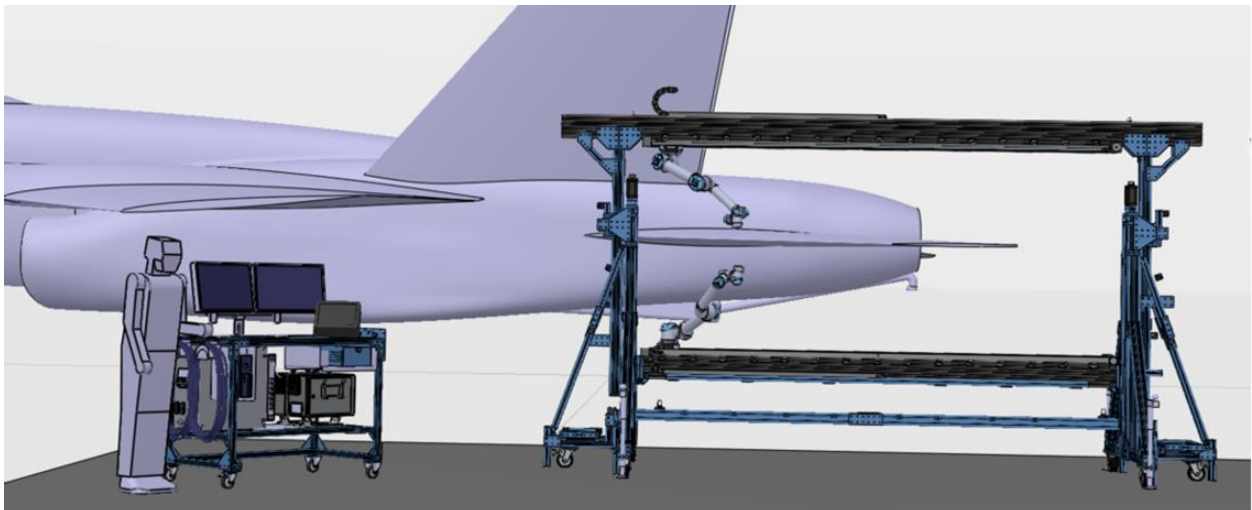
Figure 34 In-Situ Robotized Inspection

6.2 Probability of Detection of Manual and Automated Tap Testing for Disbond Detection in Honeycomb Structures

Marc Genest, Shashank Pant, Muzibur Khan, Dmitrii Klishch, Catalin Mandache, NRC Aerospace

NRC completed a Probability of Detection (PoD) study carried out for detecting disbonds on honeycomb panels using manual and automated tap testing techniques. Eight test panels containing a total of 70 different damage sites that included dents, disbonds as well as combined dent and disbonds were inspected by 11 inspectors using both manual and automated tap testing techniques. All inspectors were provided with the same experimenter briefing package before carrying out the experiment. A "hit-miss" PoD analysis was performed using all the data acquired from the inspectors.

The PoD analysis results show that the manual inspection yielded an average of 48 hits and 21 misses per inspector and a total of 43 false calls; while the automated inspection yielded an average of 51 hits, 18 misses and a total of 30 false calls. The false calls that coincide with a dent only locations were 15 for the manual tap test, and 20 for the automated tap test. It was noticed that several of the false calls obtained with the automated tap test came from values close to the threshold of 0.32, as provided in the information package. By increasing the threshold to 0.34, the number of false calls were reduced from 30 to 13, averaging 1.1 false call per inspector, and only 6 caused by dent-only damage, with the majority of inspectors having 0 false calls. However, it also increased the number of misses by 16, for an average of 50 hits and 19 misses, which remains better than manual tap testing. Although the performance of automated tap testing is overall better, it did not result in reduction of inspection time; as both manual and automated tap testing took similar amounts of time to carry out.

Overall, the a90/95 value decreased by 0.6 inch equivalent diameter using the automated tap test as compared to manual tap testing (from 1.70 to 1.10 inches). Moreover, it is important to note that inspections were carried out in ideal laboratory conditions and that the advantage of the automated tap tester over the manual tap test would likely be even more significant in noisy hangar like environments.

The reduction in false calls, up to 3 times less, obtained using the automated tap test as compared to the manual test, shows promise and is a reasonable justification to employ automated tap testing. In the worst case, even if inspectors are reluctant to changes, it would be a good tool to confirm findings obtained by manual tap testing, which could significantly reduce the number of false calls and resulting aircraft downtime.
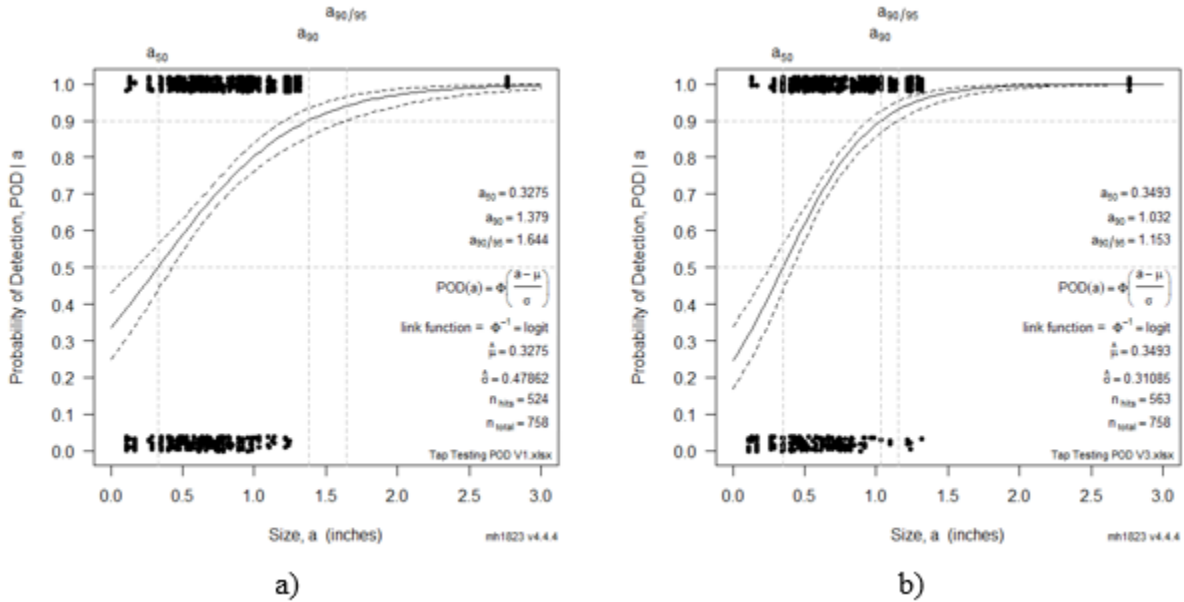
Figure 35 PoD curve cumulative for a) manual tap test; and b) automated tap test data

6.2.1 REFERENCES

[13] Muzibur Khan, Marc Genest, Shashank Pant, Dmitrii Klishch, and Catalin Mandache, "Reliability and Performance Evaluation of Manual and Automated of Tap Testing for Disbond Detection in Honeycomb Structures" Canadian Aeronautics and Space Institute Aero 2021 Conference, June 14-18, 2021

[14] Muzibur Khan, Marc Genest, Shashank Pant, Dmitrii Klishch, and Catalin Mandache, "Probability of Detection of Tap Testing for Disbond Detection in Aluminum Skin-Aluminum Core Honeycomb Structures" NDT of Composites, ASNT, June 22-24, 2021

6.3 Video Stabilization of Drone-Based Active Infrared Thermography Inspection

Shashank Pant[1], P. Nooralishahi[2], N. P. Avdelidis[2,3], C. Ibarra-Castanedo[2], M. Genest[1], S. Deane[3], J. J. Valdes[1], A. Zolotas[3], and X. P. V. Maldague[2]

[1] National Research Council Canada, Ottawa, ON K1A 0R6, Canada
[2] Computer Vision and Systems Laboratory (CVSL), Department of Electrical and Computer Engineering, Laval University, Quebec City, QC G1V 0A6, Canada
[3] School of Aerospace, Transport and Manufacturing, Cranfield University, Cranfield MK43 0AL, UK

Drones that can fly around an aircraft carrying several sensors, e.g., thermal and optical cameras, to inspect the parts of interest without removing them can have significant impact in reducing inspection time and cost. One of the main challenges in drone-based active InfraRed Thermography (IRT) inspection is the unexpected drone motion. Since active thermography is

mainly concerned with the analysis of thermal sequences, unexpected motions can disturb the thermal profiling and cause data misinterpretation, especially for providing an automated process pipeline of such inspections. Additionally, in the scenarios where post-analysis is intended to be conducted by an inspector, the drone's unexpected motions can increase the risk of human error, data misinterpretation and incorrect characterization of possible defects. Therefore, post-processing is required to minimize/eliminate such undesired motions using digital video stabilization techniques.

There are number of video stabilization algorithms that are readily available; however, selecting the best suited one is challenging. Therefore, to reduce the effect of such undesired motion, a digital video stabilization technique along with a proper methodology to select the best smoothing techniques were developed. The stabilization method is based on finding the motion between two consecutive frames using a features-based approach. To evaluate the performance of the video stabilization algorithms Multi-Scale Structural Similarity (MS-SSIM), reduction in undesired motion, and Blank Border (BB) were used. The stabilization and selection methods were evaluated experimentally on a Nomex honeycomb core carbon-fiber skin sandwich aircraft part containing manually crafted under-surface defects (holes) at different depths with various shapes and sizes, as shown in Figure 36. The experiments were also used to demonstrate a drone-based active thermography technique, where the drones where flown over the specimen at different heights, while acquiring optical and thermal videos. Figure 37 shows the optical and thermal frames taken at different heights, where the damage (drilled holes) can be seen in the thermal frame but not in the optical frame demonstrating drone-based active thermography for detecting damage.

Figure 36 Experimental setup (left), underside defects (middle), non-defective side (right).

Figure 37 Frames extracted from optical video (top) and corresponding thermal video (bottom) at increasing drone heights of 1.5 m, 2 m, and 3 m (from left to right, respectively) during active thermography inspection experiment.

6.3.1 **REFERENCES**

[15] Pant, S.; Nooralishahi, P.; Avdelidis, N.P.; Ibarra-Castanedo, C.; Genest, M.; Deane, S.; Valdes, J.J.; Zolotas, A.; Maldague, X.P.V. Evaluation and Selection of Video Stabilization Techniques for UAV-Based Active Infrared Thermography Application. Sensors 2021, 21, 1604. https://doi.org/10.3390/s21051604

7.0 ENVIRONMENTAL EFFECTS ON FATIGUE AND STRUCTURAL INTEGRITY

7.1 Aircraft Fuselage Corrosion Detection Using Artificial Intelligence

Jerzy Komorowski, JPWK Aerospace and Stan Matwin, Dalhousie University

Corrosion identification and repair is a vital task in aircraft maintenance to ensure their continued structural integrity. Regarding fuselage lap joints, typically, visual inspections are followed by non-destructive methodologies, which are time-consuming. The visual inspection of large areas suffers not only from subjectivity but also from the variable probability of corrosion detection that is aggravated by the multiple layers used in the fuselage construction. In this paper, we propose a methodology for automatic image-based corrosion detection of aircraft structures using deep neural networks. For machine learning, we use a dataset that consists of D-Sight Aircraft Inspection System (DAIS) images from different lap joints of Boeing and Airbus aircraft. We also employ transfer learning to overcome the shortage of aircraft corrosion images. With precision over 93%, we demonstrate that our approach detects corrosion with a precision comparable to that of trained operators, aiding to reduce the uncertainties related to operator fatigue or inadequate training. Our results indicate that our methodology can support specialists and engineers in corrosion monitoring in the aerospace industry, potentially contributing to the automation of condition-based maintenance protocols.

Work continues with additional training data and investigation of alternative machine learning approaches.
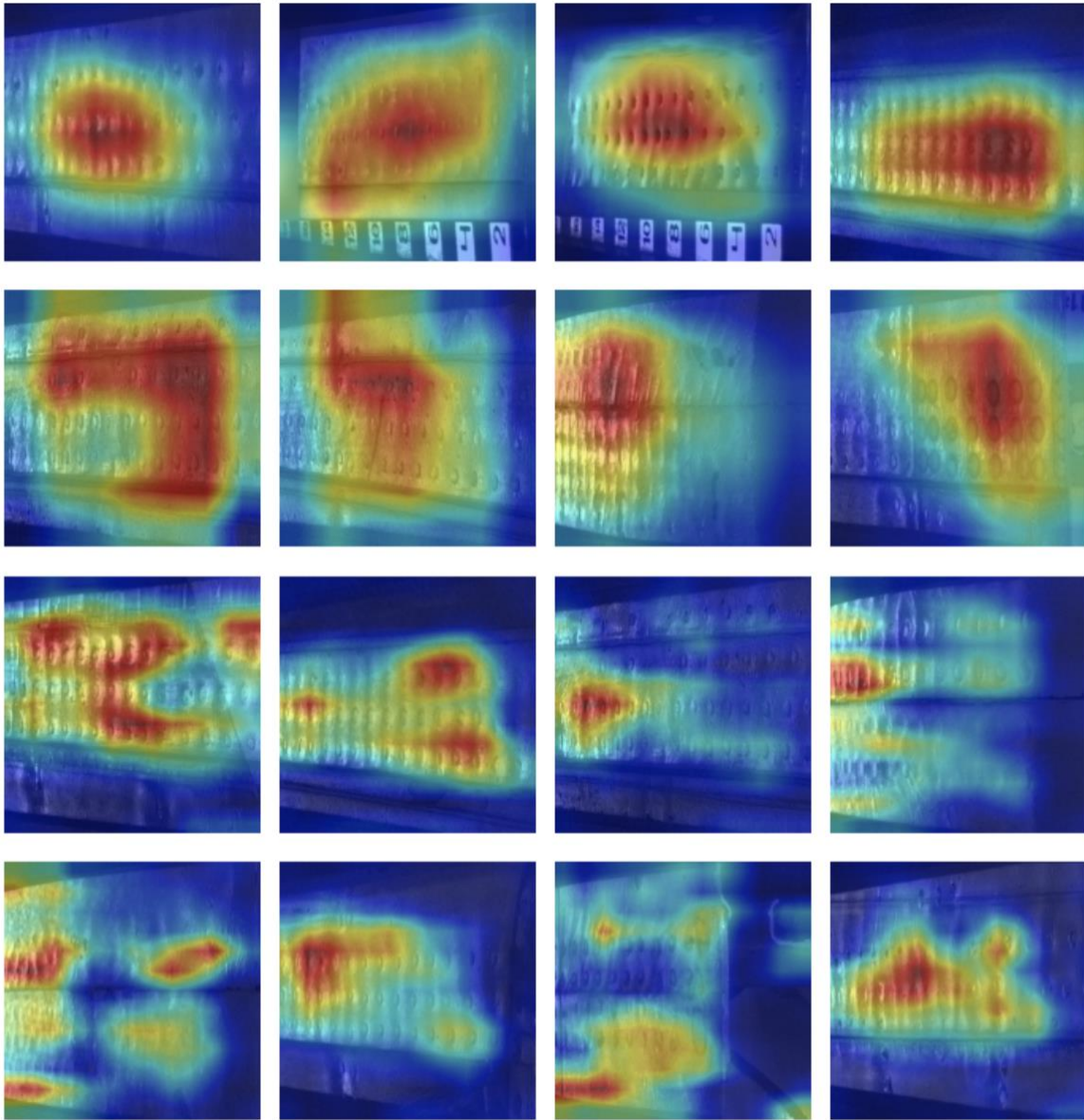
Figure 38 Visualization results through class activated maps overlaid on input true positive images together with the raw images.

7.1.1 REFERENCES

[16]   Bruno Brandoli, Andé R. De Geus, Jefferson R. Souza, Gabriel Spadon, Amilcar Soares Jr, Jose F Rodrigues Jr, Jerzy Komorowski, Stan Matwin, "Aircraft fuselage corrosion detection using artificial intelligence" Sensors 2021.

7.2 Corrosion in Aircraft Structures and Graphene-Based Sensors for Advanced Corrosion Monitoring

Lucy Li, Min Liao, NRC Aerospace

Corrosion is an ever-present phenomena of material deterioration that affects all metal structures. Timely and accurate detection of corrosion is required for structural maintenance and effective management of structural components during their life cycle. The usage of aircraft materials has been primarily driven by the need for lighter, stronger, and more robust metal alloys, rather than mitigation of corrosion. As such, the overall cost of corrosion management and aircraft downtime remains high. To illustrate, $5.67 billion or 23.6% of total sustainment costs was spent on aircraft corrosion management, as well as 14.1% of total non-available days (NAD) for US Air Force aviation and missiles in the fiscal year of 2018. The ability to detect and monitor corrosion will allow for a more efficient and cost-effective corrosion management strategy, and will therefore minimize maintenance costs and downtime, and avoid unexpected failure associated with corrosion.

Conventional and commercial efforts in corrosion detection on aircraft have focused on visual and other field detection approaches which are time- and usage-based rather than condition-based; they are also less effective in cases where the corroded area is inaccessible (e.g., fuel tanks) or hidden (rivets). The ability to target and detect specific corrosion by-products associated with the metals/metal alloys (chloride ions, fluoride ions, iron oxides, aluminium chlorides etc.), corrosion environment (pH, wetness, temperature), along with conventional approaches for physical detection of corrosion can provide early corrosion detection as well as enhanced reliability of corrosion detection. This review summarizes the state-of-art of corrosion sensing and measurement technologies for schedule-based inspections or continuous monitoring of physical, environmental and chemical presence associated with corrosion. The challenges are reviewed with regards to current gaps of corrosion detection and the complex task of corrosion management of an aircraft, with a focused overview of the corrosion factors (Figure 39) and corrosion forms that are pertinent to the aviation industry. A comprehensive overview of thin film sensing techniques for corrosion detection and monitoring on aircrafts is being conducted.

Particular attention is paid to innovative new materials, especially graphene-derived thin film sensors which rely on their ability to be configured as a conductor, semiconductor, or a functionally sensitive layer that responds to corrosion factors. Several thin film sensors have been detailed in this review as highly suited candidates for detecting corrosion through direct sensing of corrosion by-products in conjunction with the aforementioned physical and environmental corrosion parameters. The ability to print/pattern these thin film materials directly onto specific aircraft components, or deposit them onto rigid and flexible sensor surfaces and interfaces (fibre optics, microelectrode structures) make them highly suited for corrosion monitoring applications.

Advancements in chemical functionalization and patterning techniques allow for the transition toward miniaturized and monolithic sensing systems capable of monitoring multiple parameters simultaneously on a continuous basis. Furthermore, implementation of graphene derived materials in the emerging corrosion sensing techniques as presented in this review offers a wealth of possibilities for the realization of efficient and reliable real-time corrosion sensors for aircraft structural health monitoring while reducing maintenance and repair costs and maintaining the durability, sustainability, and safety of the fleets.

Figure 39 Corrosion matrix of physical, chemical and environmental factors.
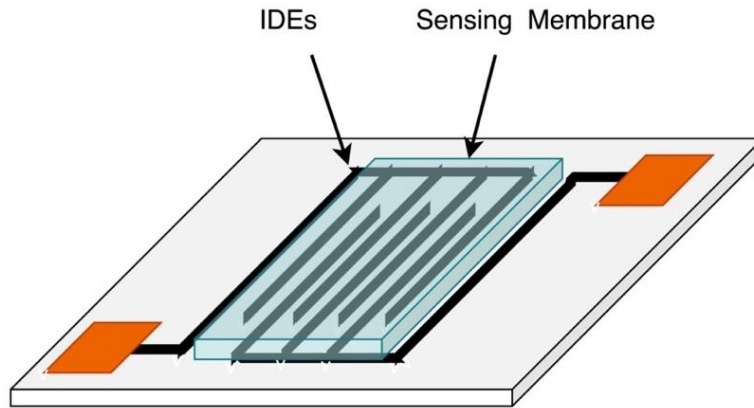
Figure 40 Schematic of an IDEs chip with PANI/CNTs conductive coating. Reproduced with permission from Rinaldi et al., Int. J. Aerospace Eng., 2012,1-11, (2012).

7.2.1 REFERENCES

[17]   Lucy Li; Chakik, M.; Prakash, R. A Review of Corrosion in Aircraft Structures and Graphene-Based, Sensors for Advanced Corrosion Monitoring. Sensors 2021, 21, 2908. https://doi.org/10.3390/s21092908

[18]   Lucy Li, Michael Menchetti, Branden Kwak, Min Liao, Prakash Patnaik, Mounia Chakik, and Ravi Prakash. Corrosion Mechanisms and Corrosion Detection of Aircraft Structures - A Review, Aerospace Research Centre, National Research Council Canada, 2021

7.3   Failure of Hot Section Components of Gas Turbine Engines & Cyclic Oxidation Test of High-temperature Protective Coatings

Kuiying Chen, NRC Aerospace

Aircraft/engine fleets experience various degradation modes and failure upon operating in harsh environments. Hot section components, such as combustor liners, turbine nozzle guide vanes and turbine blades often suffer from severe oxidation and hot corrosion attack. These damage processes will accelerate the component degradation significantly, affect engine performance, flight safety and increase maintenance costs of the fleet.

Thermal barrier coatings (TBCs) have been used to provide thermal insulation to the aero-propulsion hot section components of turbine blades and combustor liners to extend components life. The National Research Council Canada (NRC) conducted both isothermal and cyclic furnace tests, Figure 41, to evaluate TBC durability and performance and assess TBCs progressive and sequential physical damage and coating failures [19]. During thermal cycles, fatigue cracks nucleate, grow, and propagate along TBCs coating interface, leading to the final failure of TBCs.

Figure 41 CM cyclic oxidation furnace test for evaluating thermal barrier coatings durability and performance.

In addition to cycling furnace tests, NRC also conducted numerical simulations [20] to evaluate residual stresses of TBCs during thermal cycling, Figure 42 and Figure 43. The calculated residual stresses and their distribution at specific locations along the TBC interface were then used and combined with mechanics-based failure model to predict TBC life.
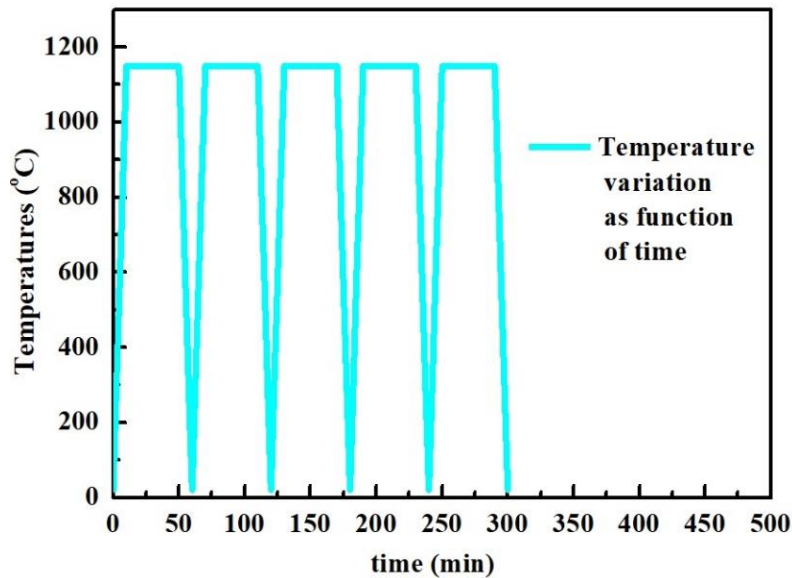
Figure 42 Temperature variation used in residual stress simulation under thermal cycling conditions.
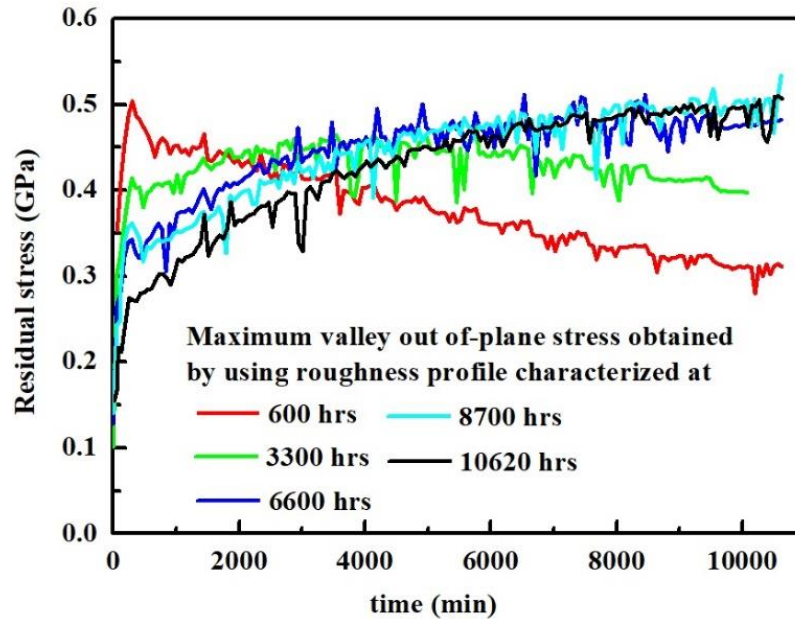
Figure 43 Out-of-plane residual stresses calculated at the valley of topcoat with different roughness profiles characterized at various stages in life cycles.

7.3.1 REFERENCES

[19] S. K. Essa, K. Chen, R. Liu, X. Wu, and M. X. Yao, "Failure Mechanisms of APS-YSZ-CoNiCrAlY Thermal Barrier Coating Under Isothermal Oxidation and Solid Particle Erosion," J. Therm. Spray Technol., 2020, doi: 10.1007/s11666-020-01124-4.

[20] B. Zhang, K. Chen, and N. Baddour, "Stress models for electron beam-physical vapor deposition thermal barrier coatings using temperature-process-dependent model parameters," J. Eur. Ceram. Soc., vol. 41, no. 11, pp. 5658–5674, 2021, doi: 10.1016/j.jeurceramsoc.2021.04.046.

8.0 FATIGUE AND STRUCTURAL INTEGRITY OF COMPOSITES

8.1 Core Damage Characterization in Aluminum Honeycomb Sandwich Panels

Diane Wowk, Royal Military College of Canada (RMC)

Honeycomb sandwich panels are commonly used for lightweight aerospace structures that require a high bending stiffness, but they can be susceptible to low-velocity impact damage. While the damage to the facesheet is visible in the form of a dent, the damage to the honeycomb core is more difficult to characterize. Studies have shown that the reduced stiffness of the crushed core is a contributing factor to local buckling of the panel during in-plane compressive loading. It is therefore necessary to be able to characterize the core damage in terms of the size and stiffness of the crumpled region.

Physical testing and dynamic numerical simulations were performed for a spherical steel ball impacting a square panel coupon with aluminum facesheets (Figure 44). The width and depth of the crumpled core was predicted and then verified through destructive sectioning. Variations in honeycomb cell size, cell wall thickness, facesheet thickness, impactor mass, impactor velocity and impactor radii were considered.
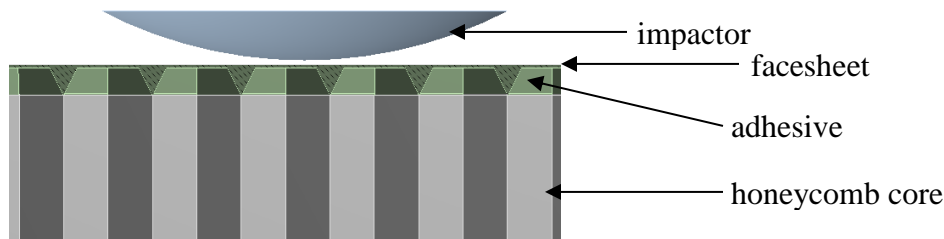
Figure 44 Components of the experimental set up and the numerical simulations.

Figure 45shows the predicted width and depth of the core damage. It was determined that for aluminum facesheets, the width of the core damage is always identical to the width of the surface dent. For dents up to 1mm in depth, the core damage depth remains the same for all panel configurations and all impact configurations as shown in Figure 46.
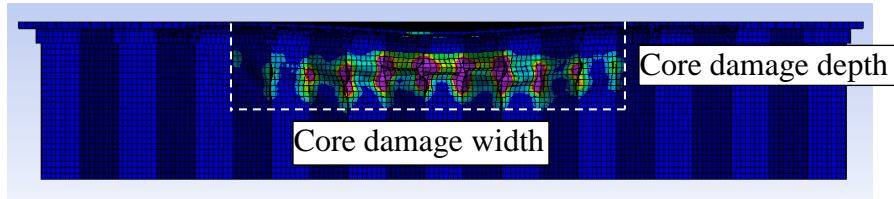
Figure 45 Numerical predictions of the width and depth of the core damage.
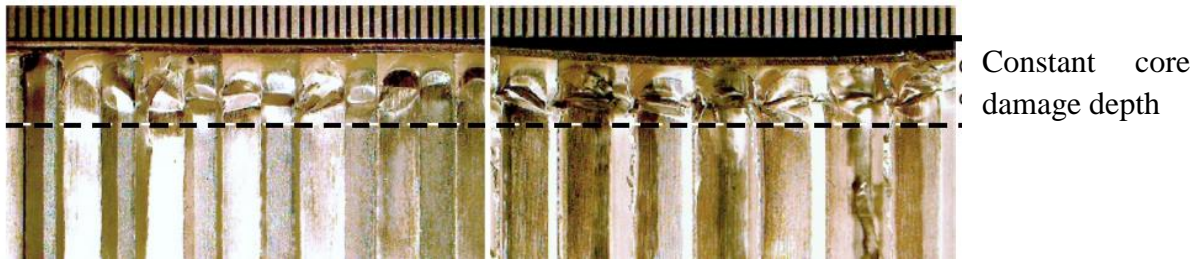
Figure 46 Core damage depth is independent of the dent depth, the impact configuration and the panel configuration.

It was shown that the only parameter that influences the depth of the core damage is the thickness of the adhesive fillets that join the cellular core to the facesheets. The adhesive fillets stabilize the tops of the cell walls and prevent them from crumpling. This causes panels with larger fillets to have core damage that is located deeper into the core as shown in Figure 47.
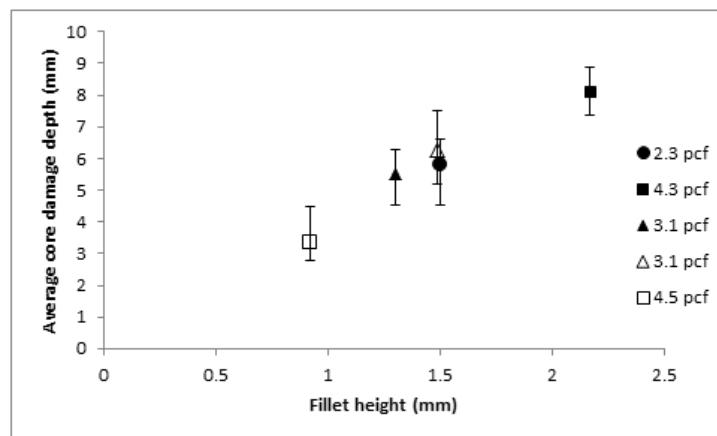
Figure 47 Physical testing showed that the core damage depth depends on the fillet height and is independent of the density of the honeycomb core (pcf).

Once crumpling of the cell walls initiates, the core in isolation (without facesheets) provides no out-of-plane stiffness as shown in Figure 48. This indicates that the resistance to local buckling of the facesheets may be reduced in the vicinity of a dent when crushed core is present.
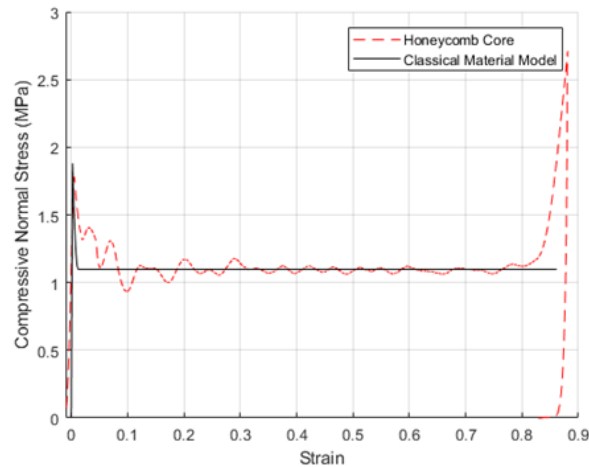
Figure 48 Stress-strain relationship for honeycomb core in isolation as compared to the idealized material model.

See the following references for more details:

8.1.1 REFERENCES

[21] Wowk D, Reyno T, Yeung R, Marsden C. An experimental and numerical investigation of core damage size in honeycomb sandwich panels subject to low-velocity impact. Composite Structures. 2020 Dec 15; 254:112739.

[22] Kendall, P. The Effects of Adhesive Quantity on Out-of-Plane Behaviour in Aluminum Honeycomb Panels". Masters thesis, Royal Military College of Canada (2019).

8.2 A Benchmarking Evaluation of Finite Element Modeling Strategies for Adhesively-Bonded Composites Using the Cohesive Zone Modeling and Virtual Crack Closure Technique

Lucy Li, Gang Qi, NRC Aerospace

Adhesive bonding has been widely used in aircraft composite structures due to its advantages over alternative joining methods. As a result, accurate predictive modelling and simulation approaches are required to optimize the design of bonded joints. The cohesive zone modelling (CZM) technique and virtual crack closure technique (VCCT) have been frequently used to predict the damage onset and evolution in adhesively-bonded composites under static and fatigue loading.

In this study, both CZM and VCCT were taken into account. First, the required material properties for the DCB model were experimentally obtained for unidirectional carbon/epoxy (G40-800/5276-1) and the adhesive (AF 163-2K). Then, the DCB modelling was performed using CZM with consideration of different stress conditions, e.g. plane strain, plane stress, and

three-dimensional, and using various element types for the beams. For each of the cases, a mesh sensitivity analysis was conducted to obtain the appropriate size of the elements. It was observed that all the approaches can obtain satisfactory results compared to the experimental results, and all the results obtained by the CZM technique were almost the same. However, the plane strain condition can give the same result with about 60% lower computation cost compared to three-dimensional configurations. Thus, for modelling adhesively-bonded DCB specimens, the suggestion is to use the plane strain condition for modelling.

Using the plane strain condition, the damage onset and propagation of the DCB specimen under quasi-static loading was also simulated by employing the VCCT approach. A force-displacement curve similar to the ones from the CZM approach was obtained. The ultimate force predicted by the VCCT was slightly higher than CZM that was deemed to be the result of elastic linear behaviour assumption in the VCCT approach. The same 2D VCCT model configuration was then used to simulate the DCB specimen under a fatigue loading condition. It was observed that this VCCT model can predict the fatigue crack growth rate of the bonded composite joints reasonably well.

While the aforementioned simulations were conducted using Abaqus/Standard implicit solver, this study also explored the potential benefit of Abaqus/Explicit solver to reduce computational costs in predict progressive damage growth of a bonded composite joint. Although the DCB test has a quasi-static loading condition, the plane strain CZM model was used for the simulation using the explicit dynamic approach via Abaqus/Explicit. To reduce the run time, mass scaling and a higher displacement rate were carefully selected. As a result, it shows that Abaqus/Explicit can also achieve the same solution accuracies as Abaqus/Standard to solve the composite failure problems, provided good modelling and solution strategies are implemented. However, contrary to expectations, usage of the explicit solver comes with a higher computational cost.
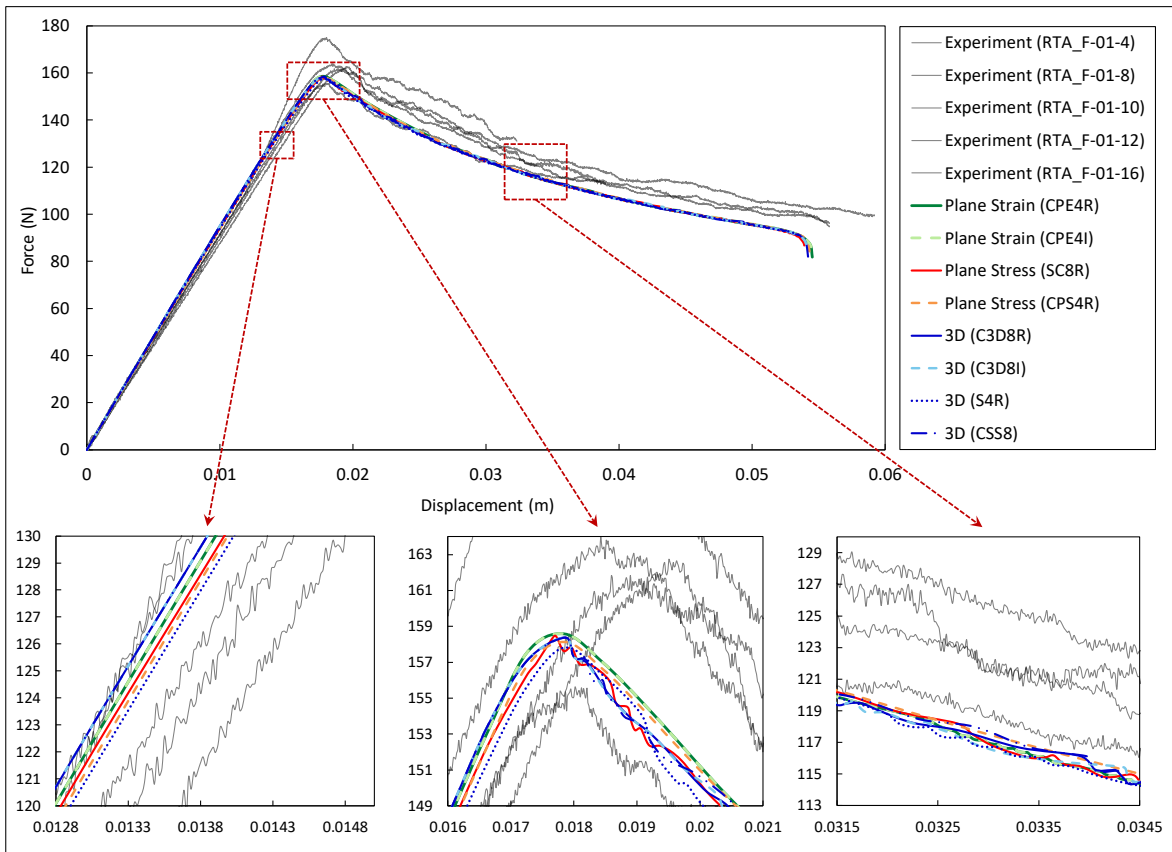
Figure 49 A comparison between the finite element analysis (CZM) and experimental results.
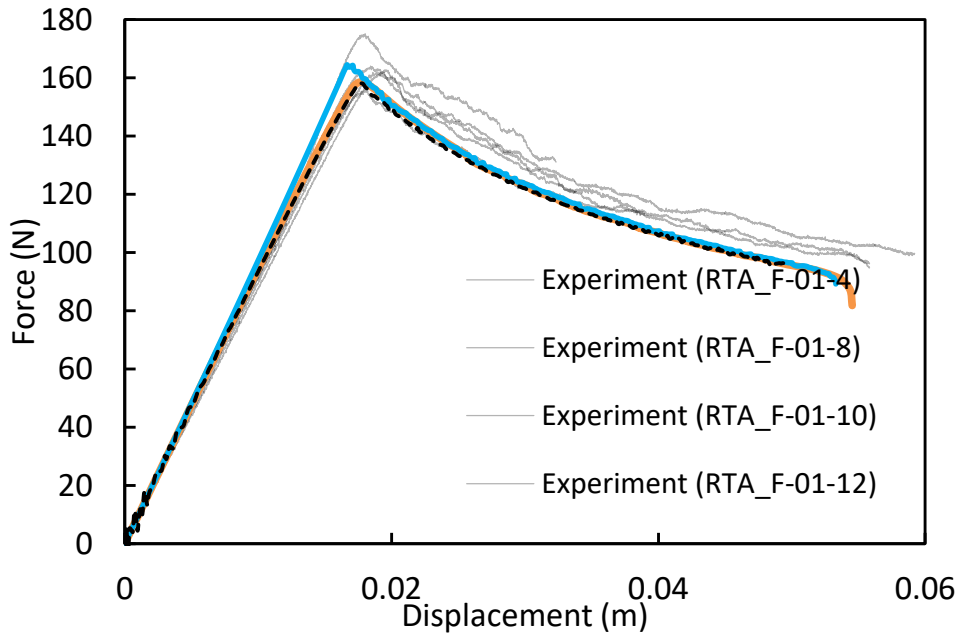
Figure 50 A comparison between the results obtained by CZM (implicit and explicit) and VCCT approaches and the experimental results.
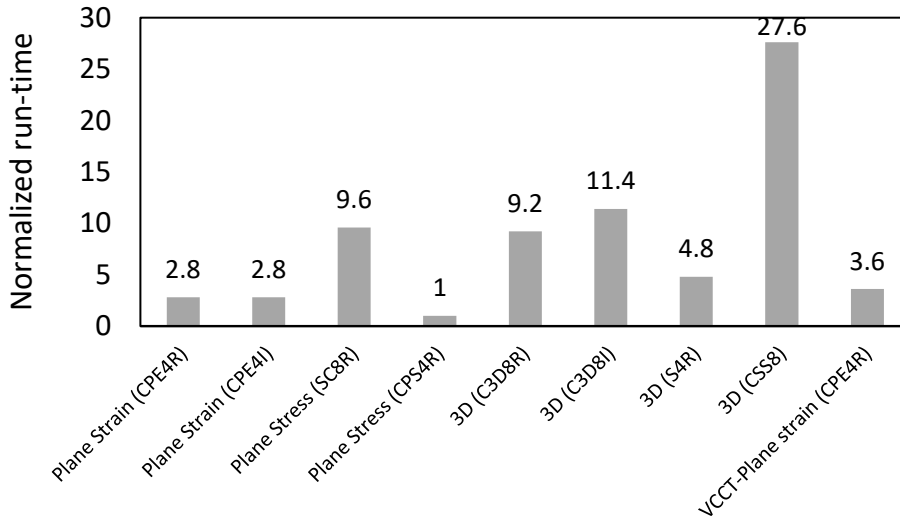
Figure 51 Normalized computation time for each of the DCB modeling approaches until δ= 0.06 m.
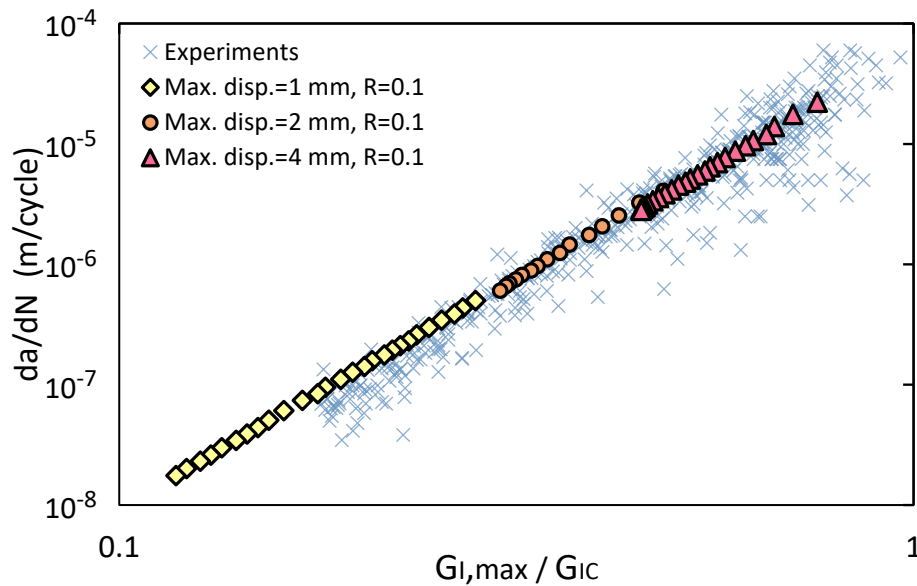
Figure 52 Fatigue crack growth rate (da/dN) versus normalized maximum strain energy release rate ($G_{I,max}/G_{IC}$). All the tests were carried out at a displacement ratio of 0.1.

8.2.1 REFERENCES

[23] Shabani, Peyman, Lucy Li, J. Laliberté, and Gang Qi. , A Benchmarking Survey On Finite Element Modeling Strategies For Adhesively-Bonded Composites Using The Cohesive Zone Modeling Technique, The 8th International Conference On The Fatigue Of Composites (ICFC8), Online, 23-25 June 2021.

[24] Li G, Li C. Linking bilinear traction law parameters to cohesive zone length for laminated composites and bonded joints. Advances in aircraft and spacecraft science. 2014 Apr;1(2):177.

[25] Li G, Li C. Assessment of debond simulation and cohesive zone length in a bonded composite joint. Composites Part B: Engineering. 2015 Feb 1; 69:359-68.

8.3 Cohesive Parameter Estimation for a Bilinear Traction-Separation Law to study DCB Mode I Failure Behaviour

Gang Li, NRC Aerospace

In this study, analytical estimation of the cohesive stiffness and strength in a bilinear traction law was conducted in conjunction with DCB Mode I test data. The developed analytical methodology was based on classical beam models and DCB deformation characteristics. A zero-thickness elastic foundation containing two layers was assumed. This elastic foundation effectively eliminates drawbacks caused by the rigid thickness assumption of the classic beam theory on the deflection analysis. The total deflection was comprised of three contributions: lateral shearing; DCB thickness deformation characteristics; and beam bending. Consequently, a significantly improved

accuracy of derived cohesive parameters was obtained. The methodology was evaluated using numerical results obtained from a 2D plane strain DCB finite element model. Good agreement was obtained between the FE and closed-form solutions for beam deflections especially at the crack tip position, and between the empirical and derived cohesive parameters. The used augmented DCB analysis model and the comparison of the derived cohesive parameters are shown in Figure 53. The four deflection conditions used in the analytical analyses were: (i) only bending, (ii) bending and lateral shear, (iii) bending and rotation caused by lateral elasticity, and (iv) the proposed methodology. Then, this method was applied to assess two DCB test cases and explored the effects of three specific factors, elastic limit load, displacement, and the initial crack length, on the two cohesive parameters, stiffness and strength. Based upon this work the proposed method theoretically explains why different cohesive parameters could lead to similar load-displacement results obtained numerically. Discussion on the agreement between the derived and the suggested cohesive values is presented along with recommendations on the application of the proposed analytical methodology.

(a)

(b)
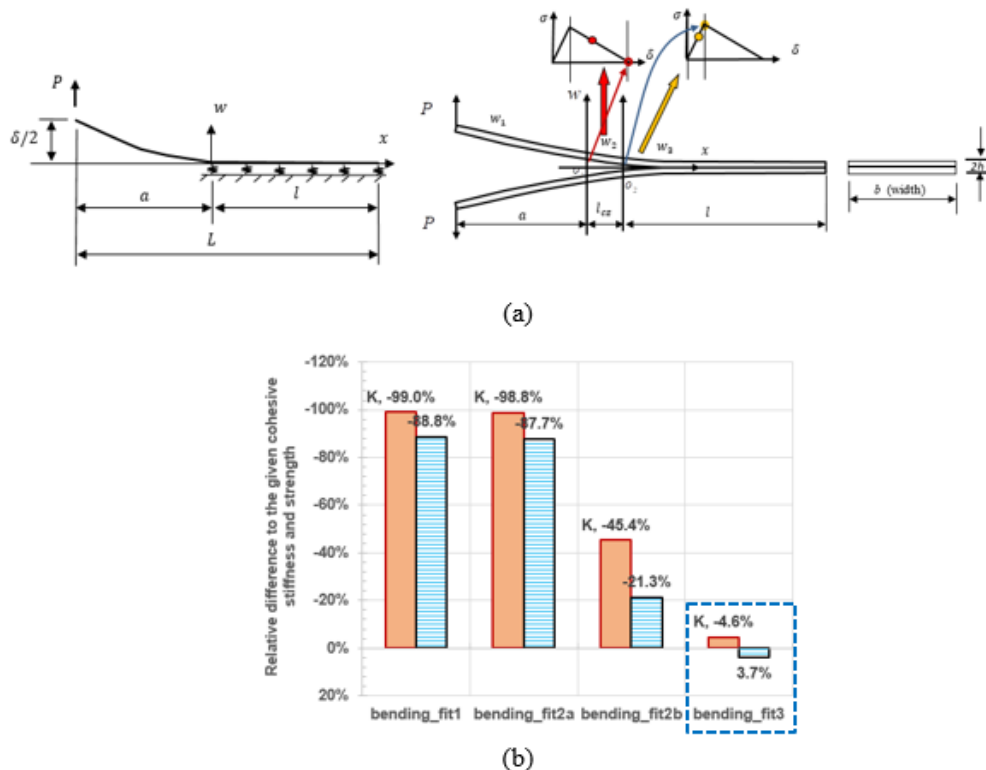
Figure 53 Schematic representation of: (a) the augmented double cantilever beam model for mode I loading, and (b) relative differences of the derived cohesive parameters to empirical values obtained from four conditions; where the "bending_fit3" refers to the proposed solution, where the orange column refers to the stiffness and the blue column represents the cohesive strength.

8.3.1 REFERENCES

[26]   G. Li, G. Renaud, M. Liao (2021), "An analysis procedure to verify delamination modelling using Cohesive elements", proceedings of 2021 AIAA SciTech Forum, Virtual Event, Jan. 11- 15 & 19-21, 2021.

[27]   G. Li (2020), " Assessment of Cohesive Stiffness and Strength of a Bilinear Traction-Separation Law for Characterization of Mode I DCB Failure Behaviour", NRC Aerospace, Laboratory Technical Report, LTR-SMM-2020-0058.

[28]   G. Li, C. Li (2013), "An analytical analysis of energy release rate in bonded composite joints in a mode I condition", Composites Part B, 44,704-713.

8.4 Stepwise Mode I Fatigue Life Characterization Method for Composite Laminates and Bonded Composite Joints

Lucy Li, NRC Aerospace

Characterization of fatigue damage growth rate, *da/dN*, is essential for prediction of fatigue life of composite structures. Currently, no ASTM standards are available to specify test procedures and data reduction of fatigue damage propagation of Mode I Double Cantilever Beam (DCB) composite coupons. A stepwise test scheme was developed to characterize damage growth rate of composite Double Cantilever Beam (DCB) samples under Mode I cyclic loading. Both DCB laminate and bonded joint samples were made and tested under fatigue to produce a total fatigue curve (Figure 54) for composite laminate and bonded joints.

$$\frac{da}{dN} = C(\frac{G_{Imax}}{G_{IR}})^n$$
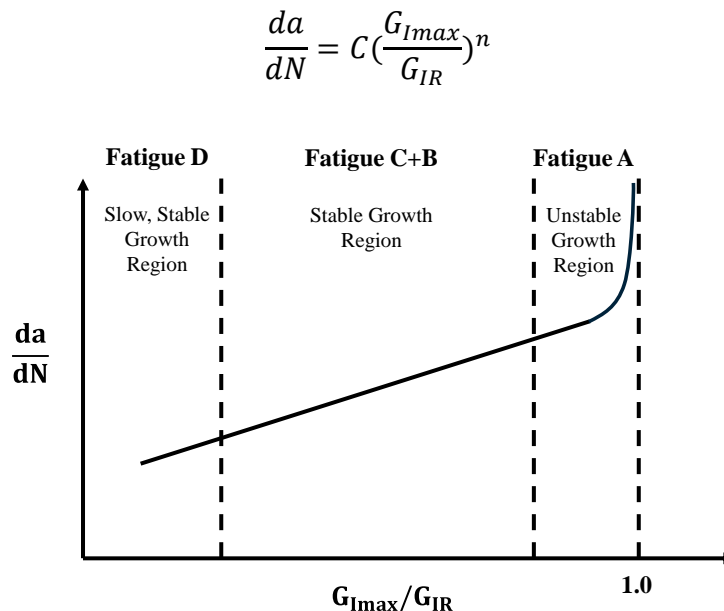
Figure 54 Schematic of fatigue damage growth curve of composites (in log scale)

To reduce the number of test samples, to reduce time, and to enhance data reliability, this step-wise fatigue test approach divides the fatigue curve into three segments, and allows for multiple fatigue tests to be conducted on a single sample. This step-wise test scheme offers several features: first, multiple fatigue tests (three for this work) are done on each single sample, starting with low to high G_{Imax}/G_{IR}, allowing fast test frequency in the slow growth region; second, a static test was conducted on each sample, which is used to take into account sample variability of G_{IR}, and also to eliminate fatigue accumulation; third, to achieve the desired G_{Imax}/G_{IR}, data training and real-time adjustment for corresponding maximum displacement could both be effective although a different curve than linear for data training is recommended tor estimating fatigue amplitude (displacement in this case); last, an in-house automated damage front monitoring system was employed in this study to collect a high volume of damage length measurements, resulting in better data reliability. This stepwise approach is recommended for Mode I fatigue curve characterization of both composite laminates and bonded joints. The fatigue life curve for the tested composite was constructed from the rate of delamination growth (da/dN) as a function of G_{Imax}/G_{IR}, as shown in Figure 55.
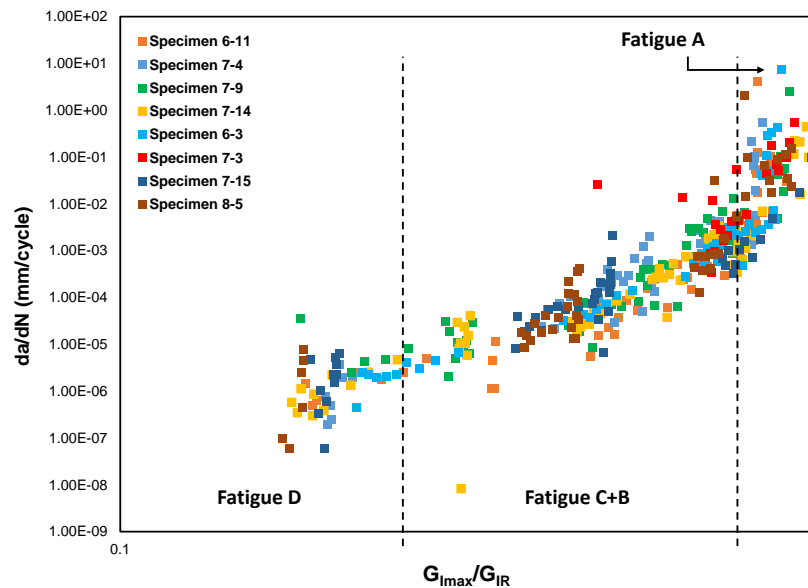
Figure 55 Preliminary results of a populated fatigue life curve

8.4.1 REFERENCES

[29]   L. Li, B. Kwak, Stepwise Mode I Fatigue Life Characterization Method for Composite Laminates and Bonded Composite Joints, The 8th International Conference On The Fatigue Of Composites (ICFC8), Online, 23-25 June 2021.

[30]   Li C., Teng T., Li G., Yanishevsky M. (2013) Fatigue Disbond Growth of Environmentally Aged/Degraded Adhesively Bonded Composite Joints under Mode I Loading, International Conference on Composite Materials, 19th International Conference on Composite Materials

[31]   Li, C., Wan, Z.Y., LaPlante, G., Rans, C., Li, G., "Long-term Durability of Adhesively Bonded Composite Joints Under Quasi-static and Fatigue Loading", Proc. 34th International Committee on Aeronautical Fatigue (ICAF) Conference and 28th ICAF Symposium, 2: 819-829, Helsinki, Finland, 2015.

9.0 FATIGUE AND STRUCTURAL INTEGRITY OF NEW MATERIAL AND MANUFACTURING

9.1 Design and Development of Additively Manufactured Aircraft Structural Components

David Backman, Priti Wanjara, Brain Sa, NRC Aerospace

In a DND sponsored project on the development and demonstration of additive manufacturing (AM) for aircraft structural application, several candidate components were discussed before deciding on a corner bracket from a Canadian flown Lockheed CP-140 Aurora. The airframe itself is based on the Lockheed P-3 Orion but utilizes the electronics suite from the Lockheed S-3 Viking. The candidate component in question is a corner (bathtub) fitting taken from the butt line (BL) 65 wing front beam lower joint [32][33].

The original component was produced from aluminum (Al) 7075-T73, but a review of the data on Al powders for additive manufacturing (AM) processes showed that current powders on the market lacked sufficient strength. As a result the decision was made to manufacture the part from titanium (Ti) 6Al-4V. An electron beam melting (EBM) machine produced by GE Additive Machines (Arcam EBM Q20+) was used to manufacture the corner fitting using a plasma atomized Grade 5 Ti-6Al-4V powder. The EBM process took place in a vacuum and at elevated temperatures, typically resulting in stress relieved components with material properties better than cast and comparable to wrought material [33].

This update summarizes the results of static and fatigue testing on the additively manufactured CP-140 corner fitting. As a component level validation of the additive manufacturing process one of the net shape fittings was machined (in the unHIP'd condition) and prepared for static testing to design limit load (17 kips) and then to ultimate load (26 kips). In addition, an overload static condition was applied to 35 kips in order to examine the weak point in the titanium AM bracket. This overload condition resulted in failure of the main bolt attaching the bracket to the lower test fixture. A new bolt was fitted to the test fixture and the AM bracket was subjected to a second round of testing to simulate a certification like test protocol. For this second round of testing, static loads to design limit load (17 kips) and ultimate limit load (26 kips) were applied and held for five seconds. Next the bracket was subjected to a 50% percentile CP-140 fatigue spectrum (FCA-301) comprising 1.16 million end levels for a total of two lifetimes of fatigue loading. The fatigue spectrum was broken up into eight blocks with marker band loading applied between each block.

A digital image correlation system was used to measure strains during static loading, with the results from design limit and ultimate load shown in Figure 56. Figure 56c shows the residual strains in the bracket post-test with no significant change in strain visible. For the fatigue portion

of the test, a microbolometer based thermoelastic stress analysis (TSA) system was used to monitor the front portion of the test while the same DIC system was used to monitor strain changes over time. In order to increase the fidelity of the strain based trend monitoring, the DIC system was triggered prior to each fatigue life time and as well at the end of each block. At the end of each fatigue block, two static load conditions were applied to the bracket (DLL and -50% DLL). These static load conditions allowed for multiple DIC images to be captured and analysed for the purpose of trend monitoring. Strains were extracted from key high strain regions in the base of the bracket at each of these load conditions. Figure 57 shows the strain changes over time for key regions at DLL while Figure 58 shows the same type of plot for key regions at -50% DLL. Overall no clear trends indicative of crack nucleation or crack propagation were evident over the first two lifetimes of fatigue testing. The microbolometer based TSA system was only setup during the later portion of the second lifetime (LC2) with the magnitude of the TSA signal shown graphically in Figure 59. In order to reduce image noise, a running average of the TSA magnitude was collected at eight second accumulation intervals. The final image prior to block end was captured and used for trend monitoring purposes. Overall, although an equipment issue resulted in a noisy image for block 7, no qualitative difference was observed between the TSA results for block 6 and block 8.

Since no crack indication was evident after static and fatigue loading to two lifetimes of usage, future testing will focus on applying additional lifetimes of fatigue loading in order to observe failure mode and location. Additional work will also focus on improving test automation with the goal of allowing the test to run unmonitored while still collecting both DIC and TSA data. The certification like process applied to this bracket suggests that the titanium replacement bracket itself has sufficient strength to meet the static and fatigue load requirements. Of potential interest in future testing is addressing whether the higher modulus of the Ti 6-4 AM material might render this part overly stiff and cause failure to transition to other portions of the CP-140 structure.
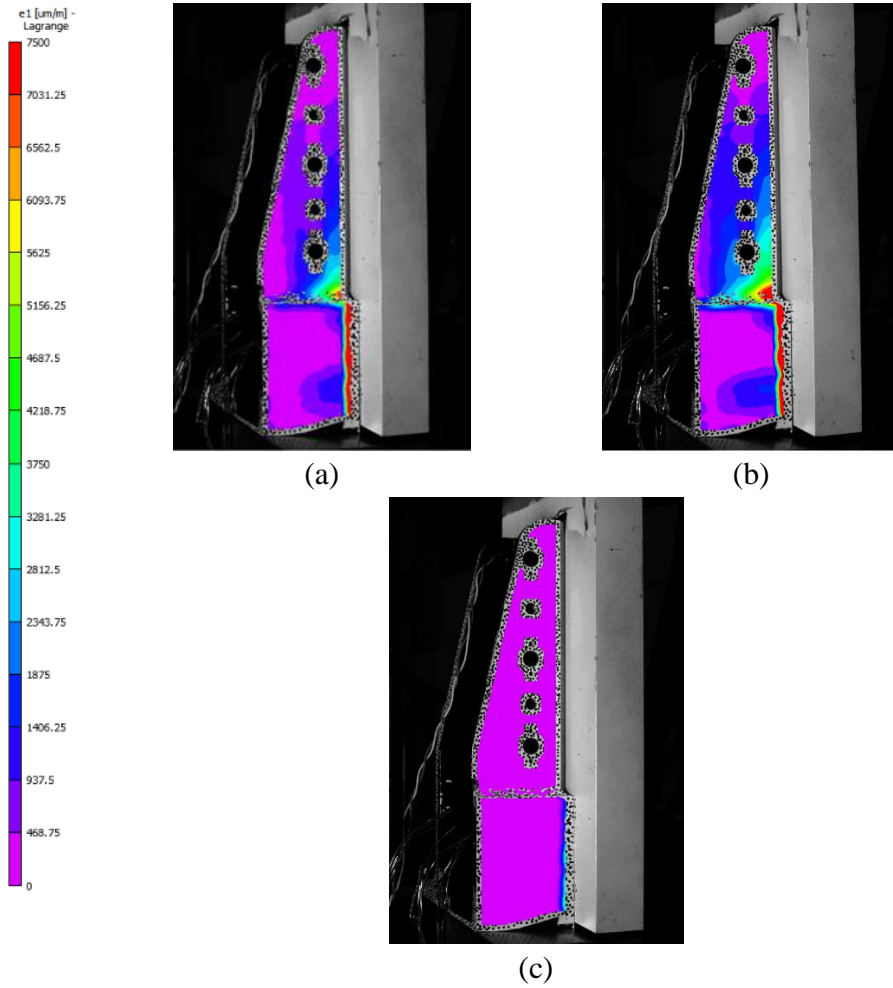
Figure 56 Static test results showing maximum principal strain from DIC at (a) 17750lbf [DLL], (b) 26500lbf [ULL] and (c) 0lbf [Post REF]
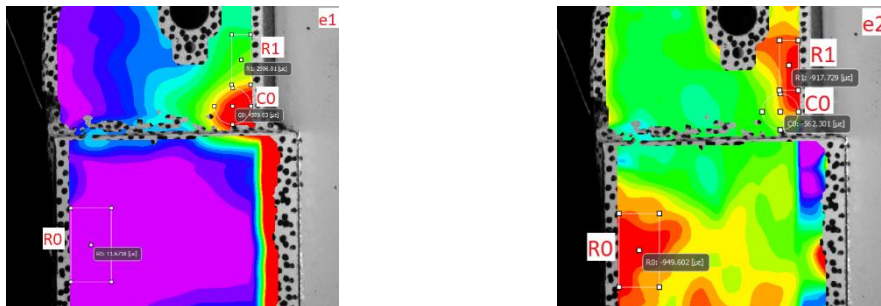
Figure 57 Trends at regions of interest from images taken at 17750lbf [DLL]
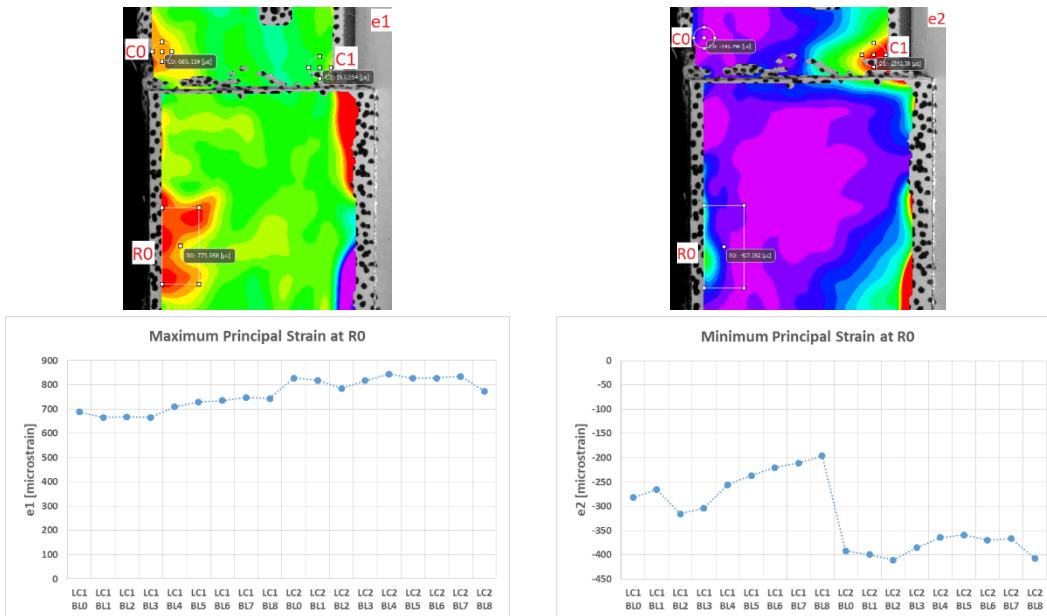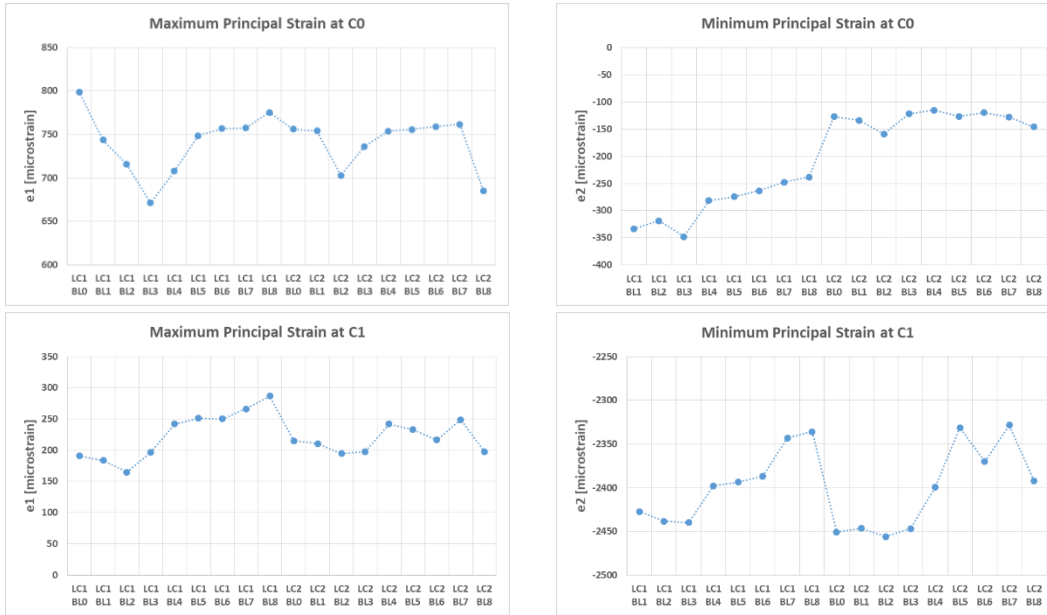
Figure 58 Trends at regions of interest from images taken at -8875lbf [-50%DLL]

LC2 BL6   LC2 BL7
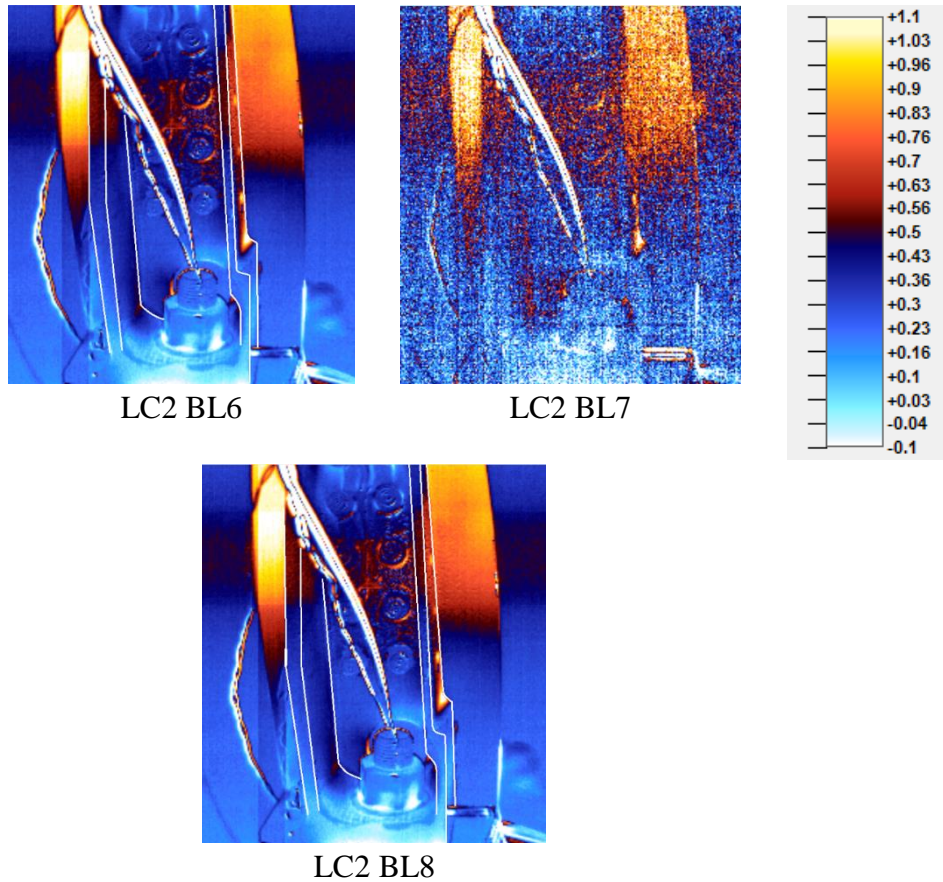
LC2 BL8

Figure 59 Magnitude of TSA signal at life cycle (LC) 2 Block (BL) 6, LC2 BL7 and the final block before test end LC2 BL8

9.1.1 REFERENCE

[32] Amos, R., Wanjara, P, Bescond, C., Backman, D., Gholipour, J., Brochu, M., Case Study: Certification of a Primary Structural Part, Canadian Aeronautics and Space Annual Conference (CASI, AERO2019), Montreal, Canada, May 2019.

[33] Liao, M., Backman, D., Gholipour, J., Wanjara, P., and Amos, R., Development and Demonstration of Additive Manufacturing for an Aircraft Structural Application, ASTM International Conference on Additive Manufacturing (ASTM ICAM 2020), November 18th, 2020.

9.2 Effect of Hot Isostatic Pressing on the mechanical properties of laser powder bed-fused Inconel 625 with intentionally-seeded porosity

Jene-Rene Poulin (NRC Aerospace), Vladimir Brailovski (École de technologie supérieure, Montreal, Canada)

Laser powder bed fusion (LPBF) is one of the additive manufacturing processes gaining significant interest from the aerospace industry. Due to the presence of processing-induced defects, mainly pores, the LPBF capacity to produce components capable of meeting stringent structural integrity requirements is often questioned. Hot isostatic pressing (HIP) is often recommended to reduce the number and size of processing-induced defects. However, some limitations of HIP have been reported, namely the difficulty to eliminate surface-connected and large irregularly-shaped lack-of-fusion (LOF) pores, which are considered to be the most detrimental from the fatigue resistance viewpoint [34]. In this context, to preserve structural integrity of LPBF components, the defect-tolerance approach appears to be more adequate than the conventional safe-life design principle [35]. To apply the former, a relationship between the size and geometry of processing-induced defects and the mechanical properties of printed components must be known.

To study the effects of HIP on the processing-induced porosity and mechanical properties of Inconel 625 LPBF components, four specimen sets (P_0, P_1, P_2, and P_3), containing four different levels of intentionally-seeded porosity ranging from $\leq 0.1\%$ to $\sim 3\%$, were manufactured. These specimens were subjected to a two-step post-processing protocol including stress relief annealing (SR) and HIP treatments, and after each treatment, the porosities as well as the tensile mechanical properties and the fatigue crack growth rates (FCGR) of the specimens were measured.

Computed tomography-based (CT) porosity measurements confirmed the efficiency of HIP in diminishing the overall porosity and the number and size of processing-induced pores. After HIP, porosity of specimens P_0, P_1 and P_2 manufactured with an initial porosity less than 1% was reduced below 0.1% (Figure 60), and this residual porosity was mainly formed by spherical near-the-surface pores. After HIP of specimens P_3 with an initial porosity of $\sim 3\%$, the residual porosity of 0.38% was mainly formed by heterogeneously distributed LOF pores (Figure 60).
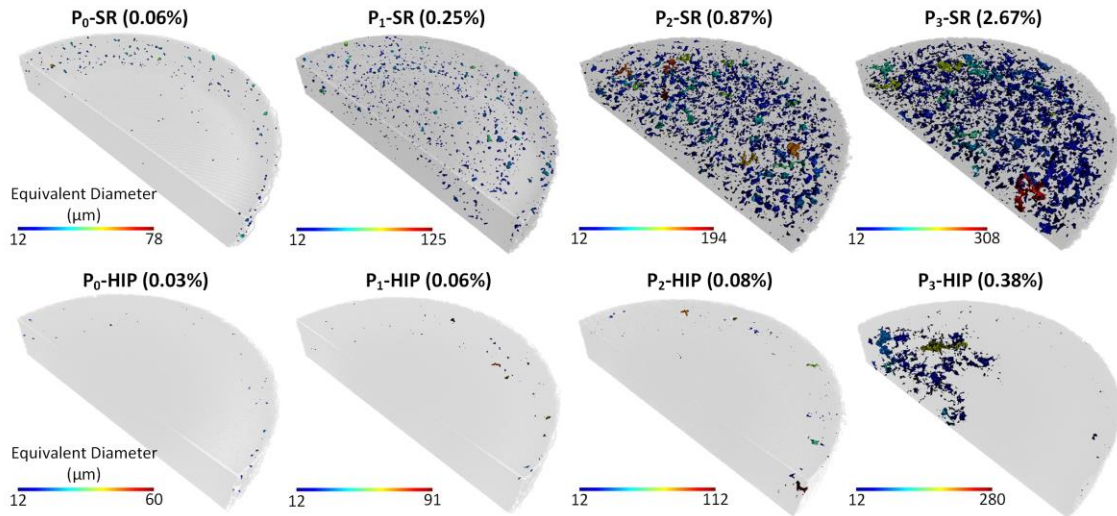
Figure 60 CT-measured porosities of specimens P0, P1, P2, and P3 after SR and SR+HIP

It is known that when the SR-ed IN625 is subjected to HIP at temperatures promoting recrystallization, delta-phase decomposes[36], which leads to a decrease in the yield stress (YS) and ultimate tensile strength (UTS) at the profit of the elongation at break (δ). The results of tensile testing shown in Figure 61 a revealed that specimens P_1 and P_2, despite a threefold difference in the as-manufactured porosity, manifest close residual porosities (0.06-0.08%) and mechanical properties ($\delta \approx 0.32$, YS ≈ 440 MPa and UTS ≈ 870 MPa). On the other hand, when the initial porosity exceeds a certain level (~1% in this study), HIP is helpful, but not sufficient to recover the inherent ductility of the alloy: δ does not exceed 0.23 for the P_3-HIP specimens.
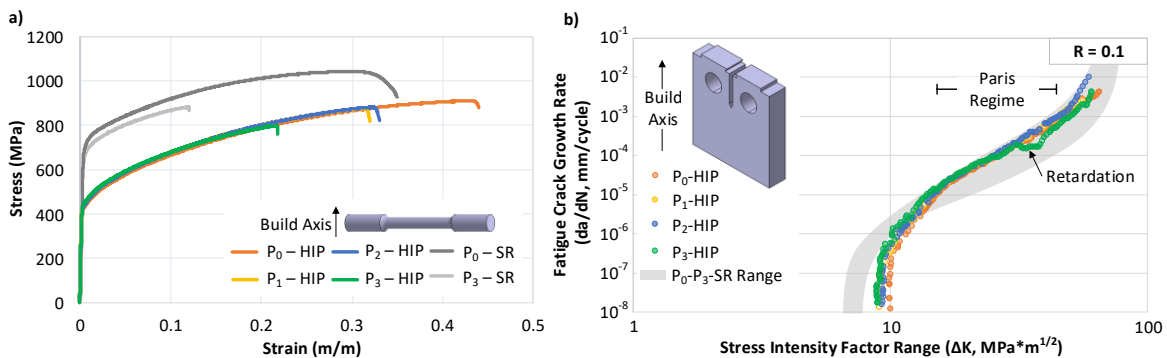
Figure 61 Mechanical properties of HIP-ed specimens: a) Stress-strain diagrams and b) FCGR diagrams; comparison is made with equivalent SR specimens [4]

The results of FCGR testing of the HIP-ed specimens were compared to those of their SR-ed equivalents taken from [37]. For all specimens, HIP led to an increase in the fatigue crack growth threshold from ~7.5 to ~9.5 MPa*m$^{1/2}$ (see Figure 61b). In the linear region of the FCGR diagrams, the fatigue crack growth rates of the HIP-ed P_0, P_1 and P_2 specimens were similar, except for the

P$_3$-HIP specimens. For the latter, the FCGR diagram deviated from the typical linear Paris-Erdogan relationship, and revealed the presence of a crack retardation event (identified in Figure 61b). The deviation coincided with the location of a large cluster of processing-induced defects typically observed for the P$_3$-HIP specimens (Figure 60). It is suggested that these defects promoted crack branching and tortuosity, and/or crack tip blunting, all of which leading to the crack retardation.

The results of this study confirm that HIP could improve the capacity of LPBF-processed IN625 components to meet stringent structural integrity requirements. However, HIP could have limited positive effect on the material properties, if the level of as-manufactured porosity exceeds ~1%.

9.2.1 REFERENCES

[34]   Yang K, Huang Q, Wang Q, Chen Q. Competing crack initiation behaviors of a laser additively manufactured nickel-based superalloy in high and very high cycle fatigue regimes. *International Journal of Fatigue.* 2020 Jul 1;136:105580.

[35]   Gorelik M. Additive manufacturing in the context of structural integrity. *International Journal of Fatigue. 2017* Jan 1;94:168-77.

[36]   Marchese G, Parizia S, Rashidi M, Saboori A, Manfredi D, Ugues D, Lombardi M, Hryha E, Biamino S. The role of texturing and microstructure evolution on the tensile behavior of heat-treated Inconel 625 produced via laser powder bed fusion. *Materials Science and Engineering: A.* 2020 Jan 2;769:138500.

[37]   Poulin JR, Kreitcberg A, Terriault P, Brailovski V. Fatigue strength prediction of laser powder bed fusion processed Inconel 625 specimens with intentionally-seeded porosity: Feasibility study. *International Journal of Fatigue.* 2020 Mar 1;132:105394.

9.3   Low Cycle Fatigue Life Prediction of a Newly-Developed Lightweight Aluminum Alloy

S.M.A.K. Mohammed[1], D.J. Li[2,*], X.Q. Zeng[2] and D.L. Chen[1]* (Corresponding author)
[1]*Department of Mechanical and Industrial Engineering, Ryerson University, Canada*
[2]*State Key Laboratory of Metal Matrix Composites, School of Materials Science and Engineering, Shanghai Jiao Tong University, China*

Prediction of fatigue life is of vital importance. Numerous fatigue life models based on either stress, strain, or energy-based calculations have been proposed to predict fatigue life of the materials and structures. Strain-controlled low cycle fatigue characteristics and energy-based fatigue life predictions were evaluated for a newly-developed Al-Mg-Si-Mn-Fe cast alloy at Ryerson University in collaboration with Shanghai Jiao Tong University [38]. The drive for increasing fuel efficiency and decreasing anthropogenic greenhouse effect via lightweighting leads to the development of new lighter Al alloys. The developed alloy exhibited superior fatigue life

owing to equiaxed fine grain morphology, fine eutectic Mg_2Si microstructure and stronger hardening capacity. Typical stress-strain hysteresis loops, following Masing behavior during mid-life cycle of specimens tested at varying strain amplitudes ranging from 0.1% to 0.8%, respectively are presented in Figure 62 (a) [38]. The hysteresis loop exhibits symmetric characteristics as a result of dislocation slip-dominated deformation in most of the face-centered cubic (FCC) materials which helps in deducing the parameters required for modeling the fatigue behavior.

The fatigue behavior was scrutinized with respect to the total strain amplitude by combination of Basquin's equation and Coffin-Mason relationship. Generally, the Basquin's equation is more suited for high cycle fatigue (HCF) regimes because the operating stresses are basically below the elastic limit, corresponding to elastic strain amplitudes ($\Delta\varepsilon_e/2$). In contrast, the Coffin-Mason relationship is used in LCF regimes where the structures are subjected to high stress and strain. Figure 62 (b), adapted from [38] shows the fatigue life summary of the as-cast Al-Mg-Si-Mn-Fe alloy in comparison with those reported in the literature, based on strain-controlled tests. No failure occurred for specimens subjected to a strain amplitude of 0.1% until 1×10^7 cycles. The run-out data points are indicated with horizontal arrows. In general, the fatigue life of the alloy decreased with increasing strain amplitude. The fact that the present die-cast alloy was free of casting defects gives rise to significantly higher fatigue and monotonic strengths, in comparison with several commercial cast and even wrought Al alloys. Despite the usual scatter in the fatigue results, the Coffin-Manson model predicted the fatigue life fairly well as can be seen in Figure 62 (c), with most of the data points lying in-between the bound lines of a factor of 1.5.
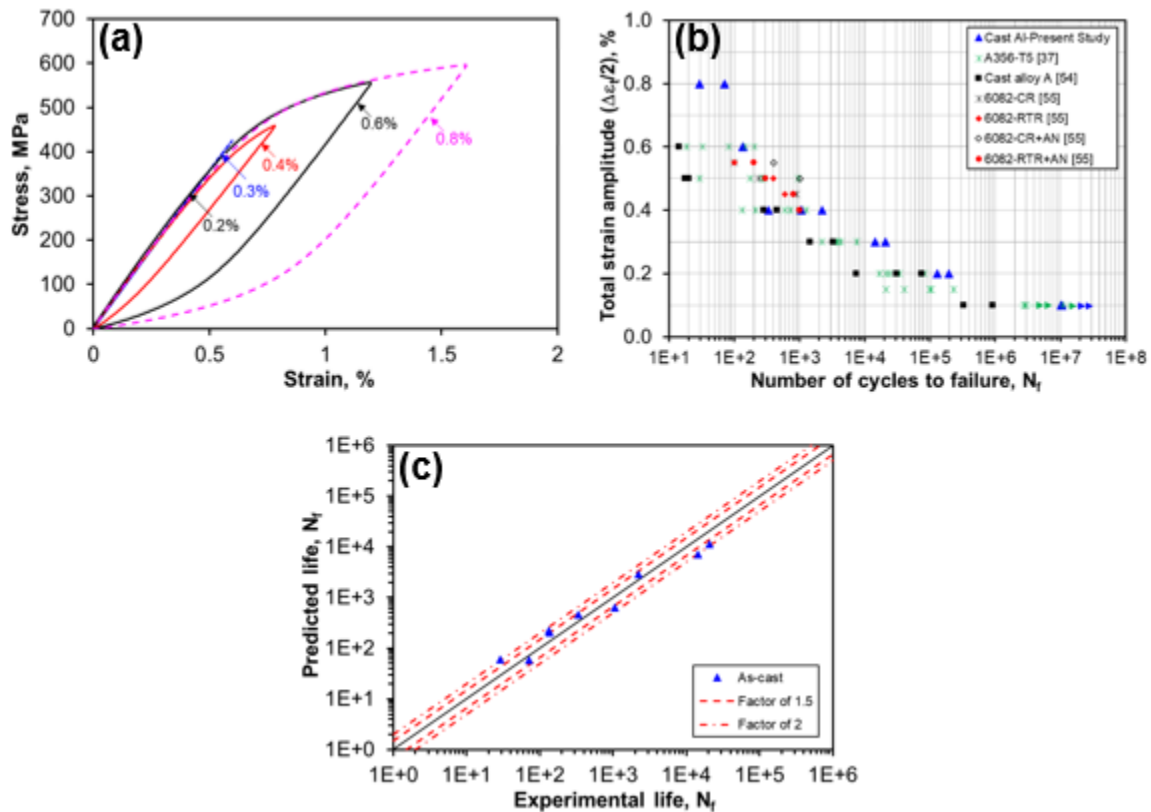
Figure 62 (a) Typical hysteresis loops at various total strain amplitudes of as-cast Al alloy during mid-life cycle following Masing behavior; (b) fatigue life summary of the as-cast Al-Mg-Si-Mn-Fe alloy in comparison with those reported in the literature; (c) predicted fatigue life vs. experimental fatigue life of the as-cast Al alloy using [38]**.**

9.3.1 REFERENCES

[38]   S.M.A.K. Mohammed, D.J. Li, X.Q. Zeng, D.L. Chen, Low-cycle fatigue behavior of a newly developed cast aluminum alloy for automotive applications, *Fatigue Fract. Eng. Mater. Struct.*, 42 (2019) 1912–1926.

9.4   Fatigue Life of a Lightweight Mg-10Zn-5Al Magnesium Alloy

S.M.A.K. Mohammed[1], D.J. Li[2,*], X.Q. Zeng[2] and D.L. Chen[1] (Corresponding author)

[1]*Department of Mechanical and Industrial Engineering, Ryerson University, Canada*

[2]*State Key Laboratory of Metal Matrix Composites, School of Materials Science and Engineering, Shanghai Jiao Tong University, China*

Fatigue life assessment tests and modeling were performed on a high zinc-containing Mg 10Zn 5Al (wt.%) cast magnesium alloy. The optimization of Zn content with a Zn/Al ratio of

~2 suppressed the presence of β-$Mg_{17}Al_{12}$ phase, and the as-cast alloy consisted mainly of primary α-Mg and eutectic-like τ-$Mg_{32}(Al, Zn)_{49}$ phase in a characteristic network form (It is worth noting that the τ-$Mg_{32}(Al, Zn)_{49}$ phase in cast magnesium alloys was first discovered by a double Nobel Prize Winner, Dr. Linus Pauling, and his colleagues in 1952 and published in a *Nature* paper entitled "Crystal structure of the intermetallic compound $Mg_{32}(Al, Zn)_{49}$ and related phases" (*Nature*, 1952, 169, 1057-1058). Symmetric hysteresis loops were observed in the investigated Mg alloy during cyclic deformation due to the absence of basal texture which caused asymmetric characteristics in the hysteresis loops. Although slight cyclic softening was reported at higher strain amplitudes, cyclic stabilization basically remained. This was also reflected by the nearly overlapped cyclic and monotonic stress-strain curves. The change of modulus of elasticity of the as-cast alloy was also noted during fatigue tests due to the existence of pseudo-elasticity or non-linear elastic behavior.

While a shorter fatigue life was observed at the higher strain amplitudes, the fatigue life of this alloy was much longer at the lower strain amplitudes, compared with several typical cast magnesium alloys, suggesting fewer cast defects present in this alloy. The strain energy-based approach could be used to predict the fatigue life. The summary of results related to the structure-process-property evaluation of the present Mg alloy adapted from [39] is presented in Figure 63. The fatigue life predicted via a strain energy-based approach was in good agreement with the experimental results. Fatigue crack initiated from the near-surface imperfections, and crack propagation was characterized by fatigue striation-like features along with tear ridges.
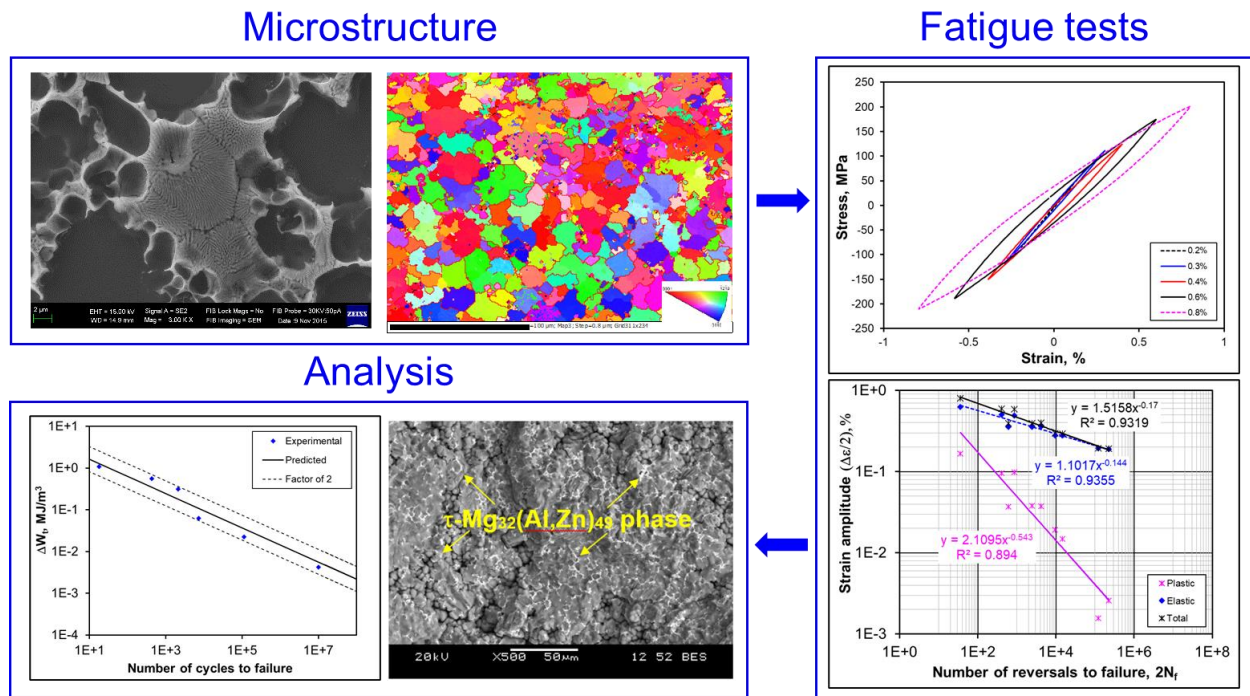
Figure 63 Summary of the microstructure and fatigue test results of a high zinc-containing Mg-10Zn-5Al cast magnesium alloy reported in [39]**.**

9.4.1 REFERENCES

[39] S.M.A.K. Mohammed, D.J. Li, X.Q. Zeng, D.L. Chen, Cyclic deformation behavior of a high zinc-containing cast magnesium alloy, *Inter. J. Fatigue*, 125 (2019) 1–10. https://doi.org/10.1016/j.ijfatigue.2019.03.015.

9.5 Fatigue Strength of an Ultrasonically Spot-Welded Clad 7075 Aluminum Alloy

S.M.A.K. Mohammed[1], Y.D. Jaya[1,2], A. Albedah[3], X.Q. Jiang[4], D.Y. Li[5], D.L. Chen[1] (Corresponding author)

[1]*Department of Mechanical and Industrial Engineering, Ryerson University, Canada*

[2]*Department of Metallurgical and Materials Engineering, National Institute of Technology, India*

[3]*Mechanical Engineering Department, College of Engineering, King Saud University, Saudi Arabia*

[4]*School of Materials and Energy, Southwest University, China*

[5]*Department of Chemical and Materials Engineering, University of Alberta, Canada*

A study on fatigue resistance and failure mode was conducted on the aerospace grade AA7075-T6 cladded with AA7072. The high-strength AA7075-T6, often specified as an "unweldable aluminum alloy" was successfully welded via solid-state ultrasonic spot welding (USW). Defect-

free sound joints were achieved with robust bonding and grain refinement via dynamic recrystallization at the weld interface, leading to superior static and fatigue properties. The failure load achieved in the joints at a weld energy of >2000 J satisfied the requirements specified in the AWS D17.2 for the spot-welded sheet specimens, with nominal tensile lap shear strength being much higher than several similar aluminum joints. The fatigue resistance was directly related to the tensile strength of the joints, and thus the so-called "unweldable AA7075" joints exhibited superior load-controlled fatigue properties as seen from Figure 64 (a) [40]. A bi-linear relationship between the maximum cyclic stress and the number of reversals to failure was present via the fitting of Basquin's equation, corresponding to different failure mechanisms: interfacial failure and transverse through-thickness (TTT) failure observed in the samples failed at the higher and lower cyclic loading levels, respectively, as shown in the insets of Figure 64 (b).

Some dimples were observed in the welded samples at higher cyclic loads as an indication of ductile failure along with fatigue failure. In general, characteristic fatigue striations were clearly observed in the samples failed at lower cyclic loads as shown in Figure 65. These observations indicated that the clad 7075 aluminum alloy could be robustly joined via solid-state USW with a superior fatigue resistance.
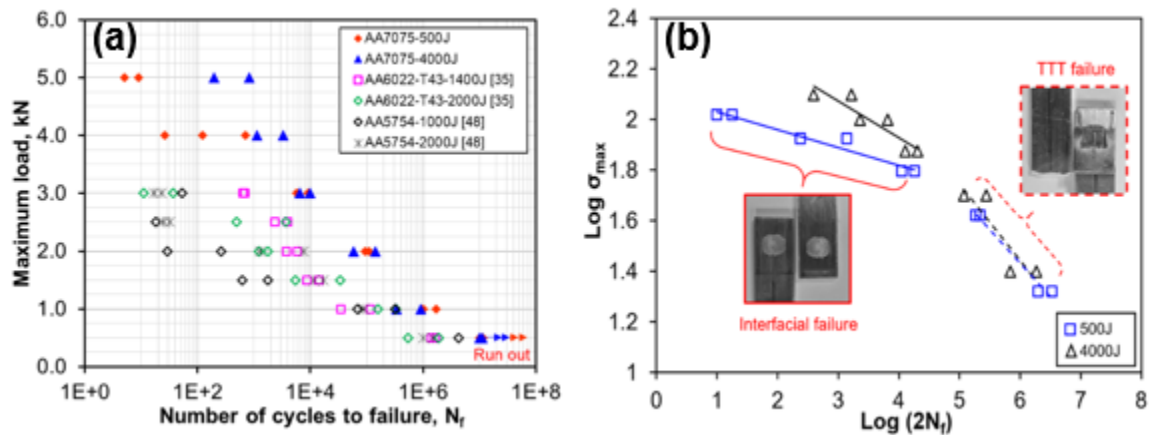
Figure 64 (a) S-N curves of the USWed AA7072-cladded AA7075-T6 joints tested at room temperature, R=0.2 and 50 Hz, along with those of USWed joints of other Al alloys, and (b) the maximum cyclic stress and the number of reversals to failure in a double-log scale [40].
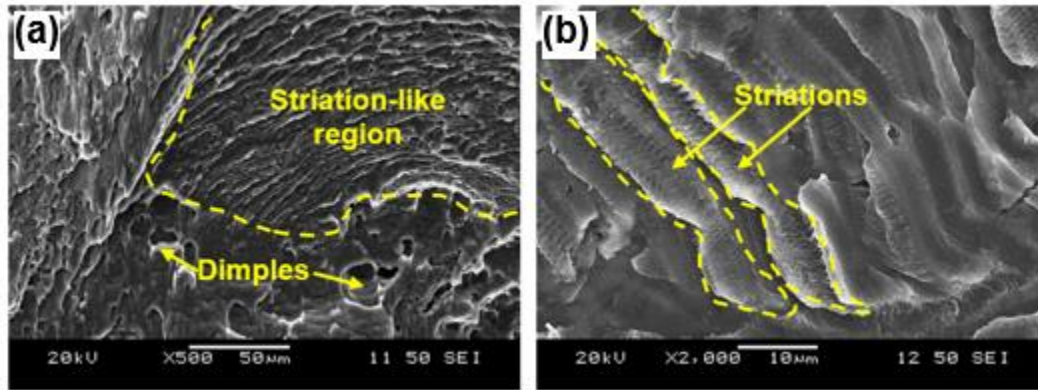
Figure 65 (a) Crack initiation site in a 500 J welded sample fatigued at P_{max} = 5 kN, and (b) crack propagation area in a 4000 J welded sample fatigued at P_{max} = 2 kN [40].

9.5.1 REFERENCES

[40] S.M.A.K. Mohammed, Y.D. Jaya, A. Albedah, X.Q. Jiang, D.Y. Li, D.L. Chen, Ultrasonic spot welding of a clad 7075 aluminum alloy: Strength and fatigue life, Inter. J. Fatigue, 141 (2020) 105869. https://doi.org/10.1016/j.ijfatigue.2020.105869.

9.6 Effect of Heat Treatment on Fatigue Behavior of an Al-Mg-Si-based Aluminum Alloy

S.M.A.K. Mohammed[1], S. Gupta[1,2], D.J. Li[3,*], X.Q. Zeng[3] D.L. Chen[1] (Corresponding author)

[1]*Department of Mechanical and Industrial Engineering, Ryerson University, Canada*

[2]*Department of Metallurgical and Materials Engineering, National Institute of Technology, India*

[3]*State Key Laboratory of Metal Matrix Composites, School of Materials Science and Engineering, Shanghai Jiao Tong University, China*

The cyclic deformation behavior of a newly-developed Al-Mg-Si-Mn-Fe alloy in the heat-treated condition was investigated at Ryerson University [41] in collaboration with Shanghai Jiao Tong University as an extension to the earlier reported work [42]. The layered (α-Al + Mg$_2$Si) eutectic structure in the as-cast condition became an in-situ Mg$_2$Si particulate-reinforced aluminum composite with spherical Mg$_2$Si particles uniformly distributed in the α-Al matrix after heat treatment. LCF tests were performed on the heat-treated alloy and compared with the as-cast counterpart. Portevin–Le Chatelier effect (also referred to as serrated flow) was observed in both tensile stress–strain curves and initial hysteresis loops (Figure 66 (a)) during cyclic deformation because of dynamic strain aging caused by strong dislocation–precipitate interactions. The vacancies are generated due to the formation of dislocation dipole loops, which follows sequential events of jog dragging, thermal dissipation of vacancies and partial dislocation annihilation. The formation of prismatic loops from elongated loops is caused by negative climb. The process of generation and emission of vacancies is schematically illustrated in Figure 66 (b).

The plastic strain amplitude is a widely accepted physical quantity to correlate the internal microstructure of the alloy with the damage process related to fatigue resistance and fatigue life. The variation in plastic strain amplitude and stress amplitude during cyclic deformation demonstrated cyclic hardening characteristics of the alloy. A simple equation based on the stress amplitude of the first and mid-life cycles $((\Delta\sigma/2)_{first}, (\Delta\sigma/2)_{mid})$ was proposed to characterize the degree of cyclic hardening/softening (D): $D = \pm \frac{(\Delta\sigma/2)_{mid} - (\Delta\sigma/2)_{first}}{(\Delta\sigma/2)_{first}}$, where the positive sign "+" represents cyclic hardening and the negative sign "−" reflects cyclic softening. The summary of fatigue life results in Figure 66 (c) reveals superior fatigue properties of the present aluminum alloy in both as-cast and heat-treated conditions compared with several commercial aluminum alloys.

Figure 66 (a) Typical hysteresis loops of the alloy in the as-cast and heat-treated states at various total strain amplitudes for the first cycle; (b) schematic representation of formation of precipitates during cyclic deformation; (c) fatigue life of heat-treated Al alloy in comparison with that of other alloys reported in the literature [41].

9.6.1 **REFERENCES**

[41]   S.M.A.K. Mohammed, S. Gupta, D.J. Li, X.Q. Zeng, D.L. Chen, Cyclic deformation behavior of a heat-treated die-cast Al-Mg-Si-based aluminum alloy, Materials, 13 (2020) 4115.

[42]   S.M.A.K. Mohammed, D.J. Li, X.Q. Zeng, D.L. Chen, Low-cycle fatigue behavior of a newly developed cast aluminum alloy for automotive applications, Fatigue Fract. Eng. Mater. Struct. 42 (2019) 1912–1926.

9.7   Low-Cycle Fatigue Life of Continuously Cyclic-Hardening Material

Zhong Zhang and Xijia Wu, NRC Aerospace

To deal with fatigue life prediction for materials with cyclically evolving stress-strain behaviours such as cyclic hardening/softening, a general fatigue life equation was derived by modifying the Tanaka-Mura-Wu dislocation pile-up model for variable strain-amplitude fatigue processes, where the fatigue crack nucleation life is expressed in terms of the root mean square of plastic strain range [43]. Low-cycle fatigue tests were conducted on an austenitic stainless steel to validate the model. At 400 °C and 600 °C, the material exhibited continuously cyclic-hardening behaviour, Figure 67. The root mean square of plastic strain ranges was evaluated from the experimental data for each test condition at strain rates ranging from 0.0002/s to 0.02/s. The variable-amplitude Tanaka-Mura-Wu model was found to be in good agreement with the LCF data, which effectively proves Miner's rule on the stored plastic strain energy basis, Figure 68.
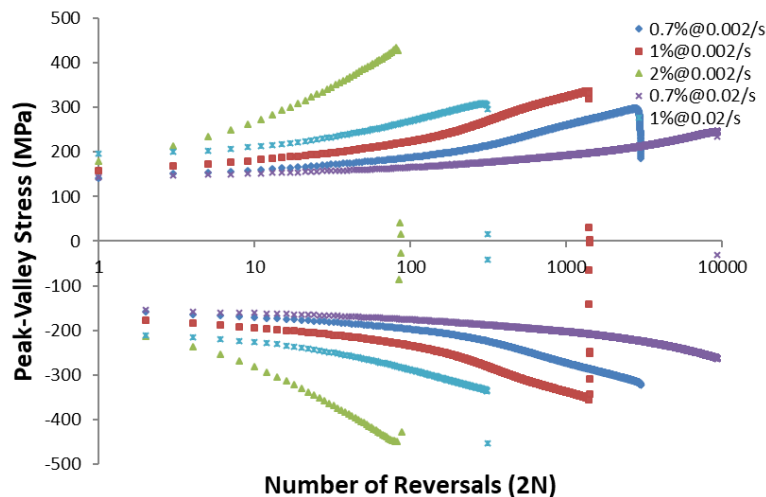
Figure 67 Cyclic peak-valley stresses of austenitic cast steel at 600°C.
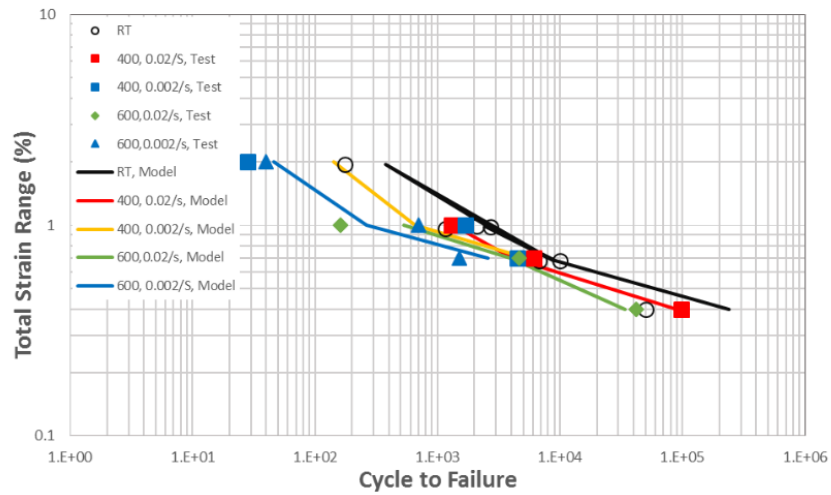
Figure 68 The total strain range vs. fatigue life for 1.4848 austenitic cast stainless steel.

9.7.1 REFERENCES

[43]   Z. Zhang and X.J. Wu, Low-cycle fatigue life of continuously cyclic-hardening material, Journal of Engineering for Gas Turbine Power, 2021, Vol. 143 / 051021.

10.0   ACKNOWLEDGEMENTS